


# Coastal occupation and foraging during the last glacial maximum and early Holocene at Waterfall Bluff, eastern Pondoland, South Africa

Erich C. Fisher<sup>a,b,c,\*</sup> , Hayley C. Cawthra<sup>b,d</sup>, Irene Esteban<sup>b,c</sup>, Antonieta Jerardino<sup>e</sup>, Frank H. Neumann<sup>c</sup>, Annette Oertle<sup>f</sup>, Justin Pargeter<sup>g,h</sup>, Rosaria B. Saktura<sup>i</sup>, Katherine Szabó<sup>j,k</sup>, Stephan Winkler<sup>l</sup>, Irit Zohar<sup>m,n</sup>

<sup>a</sup>Institute of Human Origins, School of Human Evolution and Social Change, Arizona State University, Tempe, USA

<sup>b</sup>African Centre for Coastal Palaeoscience, Nelson Mandela University, Port Elizabeth, South Africa

<sup>c</sup>Evolutionary Studies Institute, University of the Witwatersrand, Johannesburg, South Africa

<sup>d</sup>Geophysics and Remote Sensing Unit, Council for Geoscience Western Cape regional office, Cape Town, South Africa

<sup>e</sup>Department of Anthropology and Archaeology, School of Humanities, University of South Africa, Pretoria, South Africa

<sup>f</sup>Department of Archaeology, Faculty of Arts and Social Science, School of Philosophical and Historical Inquiry, University of Sydney, Sydney, Australia

<sup>g</sup>Department of Anthropology, New York University, NY, USA

<sup>h</sup>Rock Art Research Institute, School of Geography, Archaeology, and Environmental Sciences, University of the Witwatersrand, Johannesburg, South Africa

<sup>i</sup>Centre for Archaeological Science, School of Earth, Atmospheric, and Life Sciences, University of Wollongong, NSW, Australia

<sup>j</sup>Monash Indigenous Studies Centre, Monash University, Clayton VIC3800, Australia

<sup>k</sup>Museum of Archaeology and Anthropology, University of Cambridge, Cambridge UK

<sup>l</sup>NRF/iThemba Laboratory for Accelerator Based Sciences, Braamfontein 2001, Johannesburg, South Africa

<sup>m</sup>Beit Margolin Biological Collections, Oranim Academic College, Kiryat Tivon, Israel

<sup>n</sup>Zinman Institute of Archaeology, University of Haifa, Mount Carmel, Haifa, Israel

\* Corresponding author at: Institute of Human Origins, School of Human Evolution and Social Change, Arizona State University, Tempe, USA. E-mail address: [Erich.Fisher@asu.edu](mailto:Erich.Fisher@asu.edu) (E.C. Fisher).

(RECEIVED September 4, 2019; ACCEPTED February 28, 2020)

## Abstract

Waterfall Bluff is a rock shelter in eastern Pondoland, South Africa, adjacent to a narrow continental shelf that limited coastline movements across glacial/interglacial cycles. The archaeological deposits are characterized by well-preserved stratigraphy, faunal, and botanical remains alongside abundant stone artifacts and other materials. A comprehensive dating protocol consisting of 5 optically stimulated luminescence ages and 51 accelerator mass spectrometry <sup>14</sup>C ages shows that the record of hunter-gatherer occupations at Waterfall Bluff persisted from the late Pleistocene to the Holocene, spanning the last glacial maximum and the transition from the Pleistocene to the Holocene. Here, we provide detailed descriptions about the sedimentary sequence, chronology, and characteristics of the archaeological deposits at Waterfall Bluff. Remains of marine mollusks and marine fish also show, for the first time, that coastal foraging was a component of some hunter-gatherer groups' subsistence practices during glacial phases in the late Pleistocene. The presence of marine fish and shellfish further demonstrates that hunter-gatherers selectively targeted coastal resources from intertidal and estuarine habitats. Our results therefore underscore the idea that Pondoland's coastline remained a stable and predictable point on the landscape over the last glacial/interglacial transition being well positioned for hunter-gatherers to access resources from the nearby coastline, narrow continental shelf, and inland areas.

**KEY WORDS:** last glacial maximum; Late Pleistocene; Early Holocene; Hunter-gatherer; Coastal foraging; Fish exploitation; Shellfish; southern Africa; Pondoland; Eastern Cape Province

## INTRODUCTION

Developing robust predictions of the interrelationship between human behavior and ecological variability—and its archaeological signatures—is fundamental to

understanding human adaptive plasticity and survival (Roberts and Stewart, 2018). Toward the end of the Pleistocene, increasingly variable global climates transformed a long-standing, cyclical glacial-interglacial pattern into the relatively stable interglacial Holocene. As documented by numerous studies (Kirch, 2005; Anderson et al., 2007; Faith, 2014; Roberts et al., 2016), climatic changes during this time had major impacts on regional paleoenvironments worldwide which, in turn, influenced localized plant and animal communities. For hunter-gatherers, the impact of these

**Cite this article:** Fisher, E. C. *et al.* 2020. Coastal occupation and foraging during the last glacial maximum and early Holocene at Waterfall Bluff, eastern Pondoland, South Africa. *Quaternary Research* 1–41. <https://doi.org/10.1017/qua.2020.26>

habitat changes would have permeated all aspects of their lives, influencing their resource base for food, wood-fuel, medicines, utilitarian items, and all other daily necessities. These changes would have also impacted their gathering strategies as they adapted to changing distributions and types of resources on the landscapes. These changes included what resources were collected; where, when, and how resources were collected; and the duration and locations of encampments to strategically access resources and duration of stays.

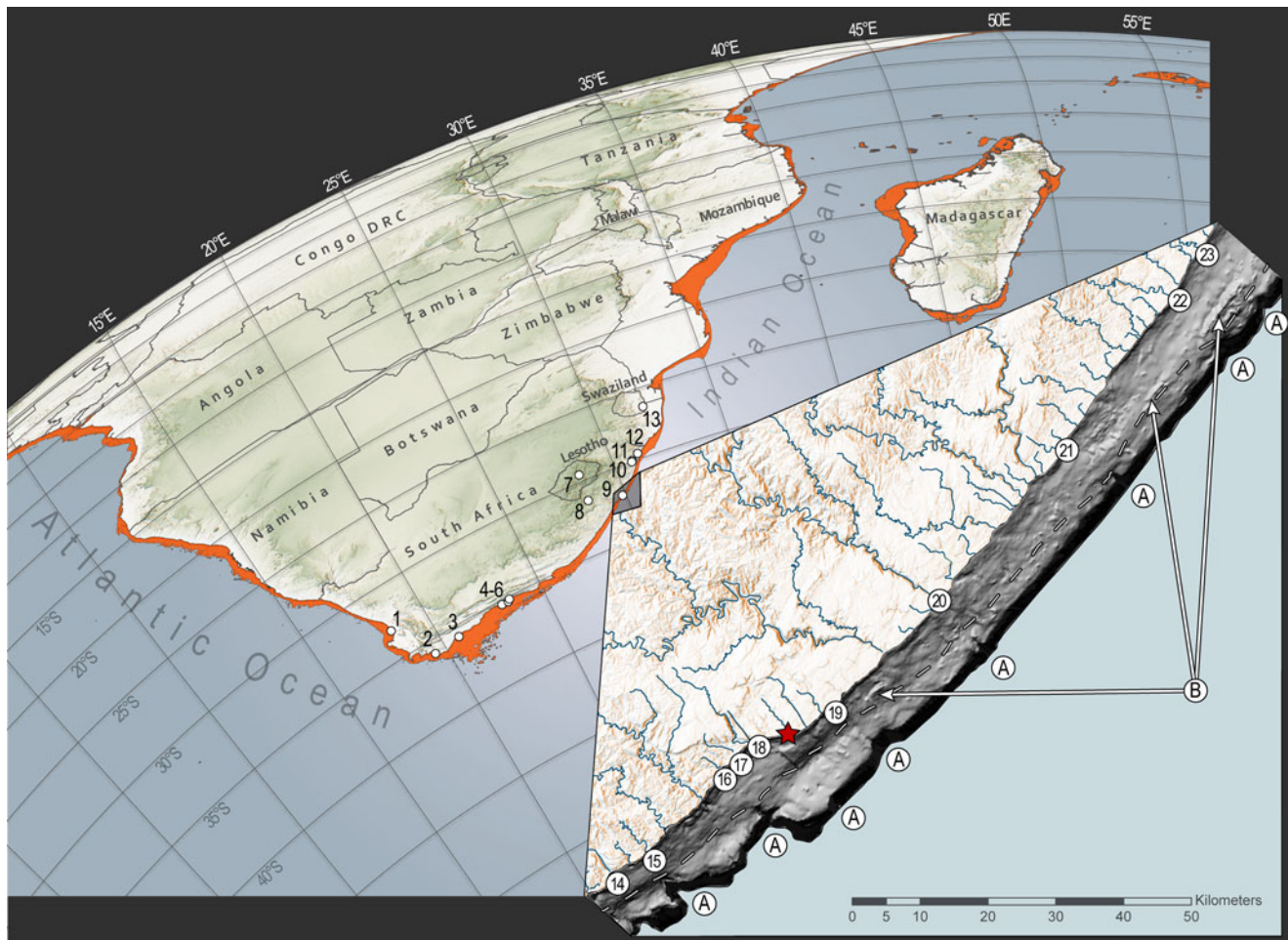
One of the most extreme habitat changes at the end of the Pleistocene occurred during the period of maximum global ice volume, known as the last glacial maximum (LGM: 26.5–19 ka; [Clark et al., 2009]). The expansion of sea ice dropped eustatic sea levels by up to 125 m below modern levels (Yokoyama et al., 2018), and these lowered sea levels exposed large tracts of land on continental margins (Fig. 1). In South Africa, geospatial models have demonstrated that upwards of 80,000 km<sup>2</sup> of seafloor was exposed across the broad and flat Agulhas Bank and Atlantic shelf—an area approximately the size of the island of Ireland today (Fisher et al., 2010). This expansive new landmass is believed to have supported populations of large grazing fauna and possibly a now-extinct migratory ecosystem (Klein, 1972, 1976; Thompson, 2010; Thompson and Henshilwood, 2011; Faith, 2013; Copeland et al., 2016; Sealy et al., 2016; Chase et al., 2018). Unfortunately, archaeological records of hunter-gatherer occupation on the continental shelf were largely destroyed by sea-level rise at the onset of Termination-I (~14 ka), leading into the Holocene (Steig et al., 1998; Heroy and Anderson, 2007; Price et al., 2007). In southern Africa, this has resulted in a near complete absence of records documenting coastal occupation and resource use dating to glacial periods. Evidence of hunter-gatherers from more inland locations shows that contemporary groups had adapted to the widespread and largely open landscapes, innovating maintainable and lightweight lithic toolkits that emphasized miniaturized freehand and bipolar core bladelet technologies (Mitchell, 1988; Pargeter et al., 2017). The presence of marine shell at some of these inland sites strongly suggests that some inland groups maintained connections to coastlines during this timeframe (Deacon, 1984; Wadley, 1993; Mitchell, 1996). What remains to be understood though is the nature of the link between shoreline and the interior, and of the communities that used these places. For instance, was there regular movement of goods and/or people between the coast and hinterland? Did some groups reside permanently at the coast? How were coastal occupations and links between coastal and interior groups influenced by climatic and environmental changes across glacial and interglacial periods?

The large changes in southern African coastlines have made it practically impossible to conduct detailed studies about how hunter-gatherers utilized coastal zones during glacial periods or across glacial-interglacial boundaries, and how these people coped with ecological variability at these times. The bulk of coastal hunter-gatherer research focuses either on

interglacial periods of the Pleistocene and the Holocene (e.g., Hendey and Volman, 1986; van Andel, 1989; Parkington, 2001, 2003, 2006, 2012; Jerardino, 2016a) or short-term sea-level transgressions during glacial phases (Marean et al., 2007). However, Fisher and colleagues (2013) hypothesized that areas with coastal caves situated adjacent to narrow continental shelves may preserve long-term and continuous records of coastal foraging, including from glacial periods. This is because narrow continental shelves would limit coastline movements so that archaeological sites found on the contemporary coastline would have been within daily or monthly coastal foraging ranges throughout glacial maxima (Fisher et al., 2010). One place of particular interest is the Pondoland region (Eastern Cape Province) on South Africa's eastern seaboard where the continental shelf is ~8 km wide. In this region, there are coastal caves incised into bedrock, numerous freshwater sources, and endemic and ancient vegetation, which make the Pondoland coastline an ideal candidate for intensive research on hunter-gatherer coastal occupation and foraging.

Here, we report on recent excavations at the site of Waterfall Bluff (formerly, A2SE-1) in eastern Pondoland where direct evidence of recurrent coastal foraging and fishing has been discovered in deposits dating to late Marine Isotope Stage (MIS) 3 (ca. 39 ka–29 ka), MIS 2 (ca. 29–14 ka), the Early Holocene (11.7–8 ka), and the Middle Holocene (ca. 8 to 5 ka). The dating of this archaeological sequence derives from 5 single-grain optically stimulated luminescence (OSL) ages and 51 accelerator mass spectrometry (AMS) <sup>14</sup>C ages, situating Waterfall Bluff among the best-dated sites of this time period in southern Africa. The MIS 2 deposits notably span the LGM (ca. 26.5–19 ka) and the last glacial/interglacial transition (LGIT: ca. 17 ka–11.7 ka) with no evident occupational or sedimentological hiatus. It is the first time that clear evidence of coastal occupation during a glacial maximum has been found in southern Africa. A companion study is providing further insights about local paleoclimatic and paleoenvironmental changes that would have directly influenced hunter-gatherer resource availability (Esteban et al. 2019). These records show varying but sustained moisture and presence of all major vegetation types found in the region today (e.g., forests, grasslands, etc.), suggesting habitable conditions and abundant resources to sustain hunter-gatherers from the end of the Pleistocene through to the Holocene. The records preserved at Waterfall Bluff, therefore, provide an unprecedented opportunity to study the role of coastal resources in hunter-gatherer diets and behavioral variability in a persistent coastal context across a glacial/interglacial cycle.

This paper describes the excavations, stratigraphic sequences, and chronology of Waterfall Bluff. It also provides a brief overview of key aspects of the marine foraging and fishing evidence, including our preliminary results from archaeomalacological, archaeoichthyofaunal, and lithic studies. These descriptions are a first step toward our long-term goal of understanding hunter-gatherer behavioral adaptations in coastal contexts across a glacial-interglacial



**Figure 1.** Archaeological sites mentioned in the text with inset showing the bathymetry of the continental shelf adjacent to Waterfall Bluff and the maximum extent of continental shelf exposure during the last glacial maximum. The main image shows archaeological sites referenced in the text and the maximum exposure of the continental shelf during the last glacial maximum. The sites are: (1) Elands Bay Cave, (2) Byneskranskop Cave, (3) Klipdrift rock shelter, (4) Knysna Eastern Heads 1, (5) Nelson Bay Cave, (6) Matjies River rock shelter, (7) Sehonghong, (8) Strathlahan B, (9) Waterfall Bluff, (10) Shongweni, (11) Umhlatuzana, (12) Sibudu Cave, and (13) Border Cave. The inset shows the bathymetric model of the seafloor around Waterfall Bluff (red star) and seafloor features in the submerged environment. The dashed line represents a prominent paleoshoreline terrace between the mid and outer shelves at  $-60$  meters. Submarine canyons from paleoriver channels (unnamed) are labeled “A.” The modern river systems that are associated with these canyon heads that impinge on the continental shelf are: (14) Mzimvubu; (15) Nkodusweni; (16) Mzimpunzi; (17) Mbotyi; (18) Mkozi Rivers; (19) Mkweni and Tezana Rivers; (20) Mtentu; (21) Kuboboyi; (22) Vunga and (23) Zotsha. Remnant paleocoastlines are labeled “B.” (For interpretation of the references to color in this figure legend, the reader is referred to the web version of this article.)

boundary and how coastal foraging fit within the broader sphere of hunter-gatherer lifeways in southern Africa.

## EASTERN PONDOLAND

### Geology and geomorphology

The fragmentation of the supercontinent Gondwana commenced in the Early Cretaceous (ca. 136 Ma) as South America was sheared westward along the Falkland Agulhas Fracture Zone (Martin and Hartnady, 1986; Eagles, 2007), creating the steep and deep shelf break on South Africa’s eastern seaboard that is now only  $\sim 8$  km wide. The unique morphology of the continental shelf plays an important role in

Pondoland’s climate and ecology, primarily by preventing the warm-water Agulhas Current from drifting too far from the coastline during the Pleistocene and Holocene (Winter and Martin, 1990; Peeters et al., 2004). The effect of the warm Agulhas Current today drives the convection of moist coastal air cells for coastal precipitation, delivering a source of fresh water to the region (Jury et al., 1993; Schumann et al., 1995). It also influences marine habitats by stabilizing inshore water temperature, which supports intertidal shellfish and littoral fish communities. Paleoceanographic records show that the Agulhas Current may have been up to  $4^{\circ}\text{C}$  cooler during the LGM (Simon et al., 2013; Simon et al., 2015a; Simon et al., 2015b), but with little variability in the location or strength of the current (Purcell, 2014). These

relatively cooler, but sustained, waters offshore Pondoland during the LGM would have continued to maintain suitable habitats for local shellfish communities, particularly those species that were harvested most frequently.

On land, the Pondoland coastline is dominated by various formations of sandstones, shales, and dolerites to the south with granites and gneisses to the north (Fig. 2). Most significant on this coast is a trapezoidal exposure of Late Devonian (385–359 Ma) Msikaba Formation sandstones (Kingsley and Marshall, 2009) that is ~70 km long × ~20 km wide. Inland lithologies beyond the coastal plain are made up of deposits of the Carboniferous to Triassic Karoo Supergroup, including bands of glacial tillites and diamictites of the Dwyka Group, Ecca Group shales, and mudstone and sandstones of the Beaufort Group. Drakensberg Group flood basalts cap the Great Escarpment, which lies ~150 km inland from the Pondoland Coast. Dolerite dykes and sills had penetrated the clastic deposits of the Karoo Supergroup at the time of extrusion of the Drakensberg Group lavas (Duncan et al., 1997).

The Msikaba sandstones are an important feature of this area because these rocks have supported the formation of coastal and riverine rock shelters, which were occupied by hunter-gatherers, and now protect fragile archaeological records, including shellfish and fish remains, that would be more susceptible to deterioration in open-air contexts. This, and the narrowness of the shelf, means that any archaeological site found on or near the modern coastline at Waterfall Bluff would have remained within daily or monthly coastal foraging ranges (5–10 km) throughout glacial maxima (Fisher et al., 2010). Pondoland, therefore, is one of the few known places across the entire South African seaboard where one can justifiably expect to find continuous records of coastal foraging and fishing that have not, or only to a lesser degree, been influenced by coastline changes.

### Pondoland climate and vegetation

Pondoland is part of the Indian Ocean Coastal Belt (IOCB) biome, a well-known center of biodiversity and plant endemism (Van Wyk, 1996; Mucina et al., 2006). Contemporary rainfall in the region is predominantly during austral summer with precipitation reaching 1,120 mm/yr (Mucina et al., 2006). Under summer rainfall conditions, the amount and character of rainfall in the IOCB is topographically dependent. The northern regions close to the coast have year-round rainfall, while rainfall seasonality increases inland. Today, our study area has one of the highest proportions of winter-rainfall among the coastal areas of the IOCB with up to 36.6% winter rainfall (Cawe, 1994; Mucina et al., 2006).

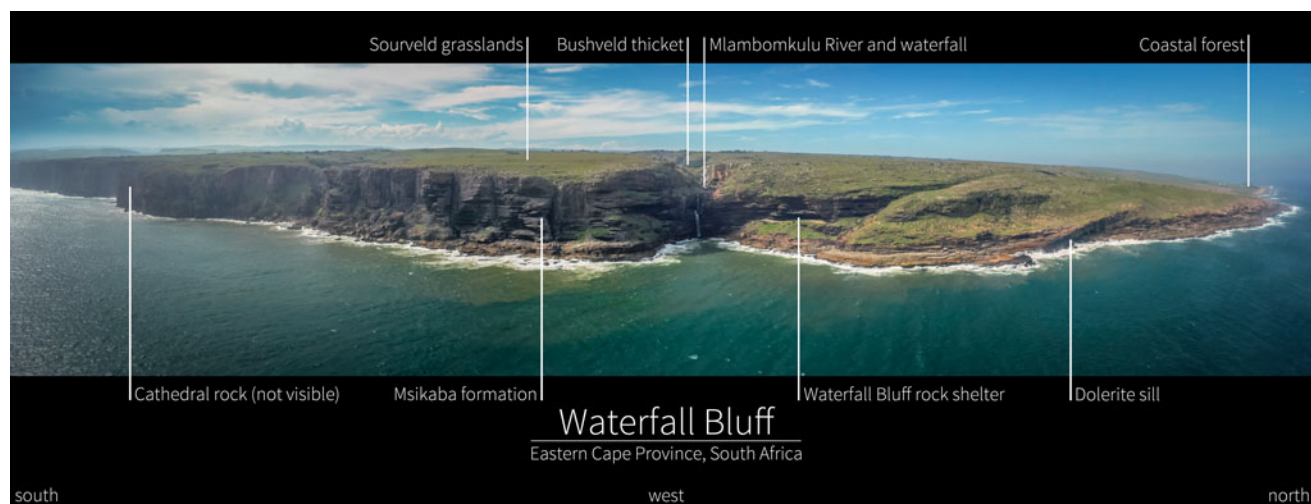
The Pondoland landscape is characterized by elevated plateaus and deep gorges. The coarse-grained Msikaba Formation sandstones have shallow, leached, acidic sandy soils (Mucina et al., 2006) that are dominated by sourveld grasslands (Pondoland-Ugu Sandstone Coastal Sourveld). Thicket vegetation (i.e., Eastern Valley Bushveld) is common in fire-resistant areas like riverine floodplains. Forests are found throughout the area and include tall, species-rich, and structurally diverse

subtropical Scarp Forests at the coast, along cliffs, and in gorges; Southern Coastal Forests along the coastline that are dominated by *Celtis africana* and *Sideroxylon inerme* (milkwood tree); and Southern Mistbelt Forests further inland at altitudes between 850 and 1100 m above sea level (Mucina and Geldenhuys, 2006) (see Fig. 2). The resilience of Scarp Forests and Afrotemperate Forests in the Eastern Cape Province and KwaZulu-Natal has made these habitats important ecosystems during glacial phases and, particularly, during the LGM (Lawes et al., 2007; Esteban et al., 2019).

### Prior archaeological research in eastern Pondoland

The ~100 km stretch of Eastern Cape coast between Port St. Johns in the South and the Mtamvuna River in the north preserves a rich archaeological record that dates back ca. 300 ka (Fisher et al., 2013; Fisher, 2016). Yet almost nothing was known about Pondoland's pre-Iron Age archaeological record before the inception of our research project. Chubb and colleagues (1934) documented excavations at a local rock shelter in 1932, and Davies reported on undated surface lithic scatters from the broader Natal region, which he attributed to the Earlier Stone Age's "Sangoan" Industry (Davies, 1976, 1982). Kuman and colleagues briefly report on extensive surface exposures of handaxes and other large bifacial tools along northern Pondoland's Red Sands area at Xolobeni (Kuman and Clarke, 2005). But apart from these preliminary reports, and the research by Feely and colleagues (Feely, 1980, 1985, 1986; Granger et al., 1985; Feely and Bell-Cross, 2011) that focused on Iron Age occupations, there are no other published accounts about the pre-Iron Age prehistory from the area. What little is known comes from sites in the surrounding region—Sibudu Cave, Border Cave, Sehanghong, Strathlahan, and Umhlatuzana—yet each of these sites is at least 350 km away from eastern Pondoland and none are coastal (see Fig. 1).

Importantly, Pondoland and the broader Eastern Cape provides observations of some of southern Africa's only historically documented mountain and coastal hunter-gatherer groups. Historical reference to hunter-gatherer groups in the Eastern Cape mention ephemeral open-air hunting camps (Vinnicombe, 1976:30). Historical records also suggest that some recent hunter-gatherer groups partook in short-term seasonal logistical forays from the nearby Maloti-Drakensberg Mountains into lowland areas of KwaZulu-Natal and the coastal lowlands of the Eastern Cape to hunt, acquire raw materials not available in the highlands, and engage in trade and stock theft from neighboring farmers (Wright, 1971). For example, the widely used plant poisons derived from *Acokanthera oblongifolia* and *Acokanthera oppositifolia*, which were common to highland hunter-gatherer groups, are species not known to occur in the Lesotho highlands but are prevalent in the vegetation of the Eastern Cape and KwaZulu-Natal Provinces (Cable, 1984). *Acokanthera* poisons are also made more toxic during the drier winter seasons, suggesting possible seasonal mobility between interior highland and coastal lowland regions (Schapera, 1923).



**Figure 2.** (color online) Low-altitude panorama of Waterfall Bluff looking westward. Taken with a DJI Mavic Pro, this image shows Waterfall Bluff, the rock shelter, and the surrounding cliffs and landscape. From left to right, the image pans from south to north, respectively.

In Africa, ethnographic examples of logistical mobility—the movement of resources to consumers, *sensu* Binford (1980)—are rare, and Marean (2016) has argued that the African archaeological record is likely to comprise a “modern human hunter–gatherer adaptive system typified by high residential mobility.” However, logistical mobility may have been more widespread than can be inferred from existing ethnographic evidence, which has been derived mainly from resource-poor environments like the Kalahari that are poorly suited to the use of logistical mobility strategies. In the cross-section between the Lesotho escarpment and the Eastern Cape coastal forelands, the available ethnographic records of recent hunter-gatherers hints at complex seasonal mobility patterns, which may themselves reflect a pattern that existed earlier in the Holocene and even the late Pleistocene. The presence of a single marine shell bead (*Nassarius kraussianus*) derived from early LGM (23,800–24,400 cal yr BP) layer BAS at Sehonghong rock shelter in Lesotho, for example, as well as numerous marine shell beads from Indian Ocean contexts in Holocene deposits certainly support this inference (Mitchell, 1996). These patterns are associated with seasonal food scarcities and the cyclical availability of resources. Few of Africa’s other ethnographic archives describe hunter-gatherers living in such conditions. A more detailed examination of Pondoland’s archaeological traces provides insight on a matter currently under-described in the ethnographic record.

### The P5 Project

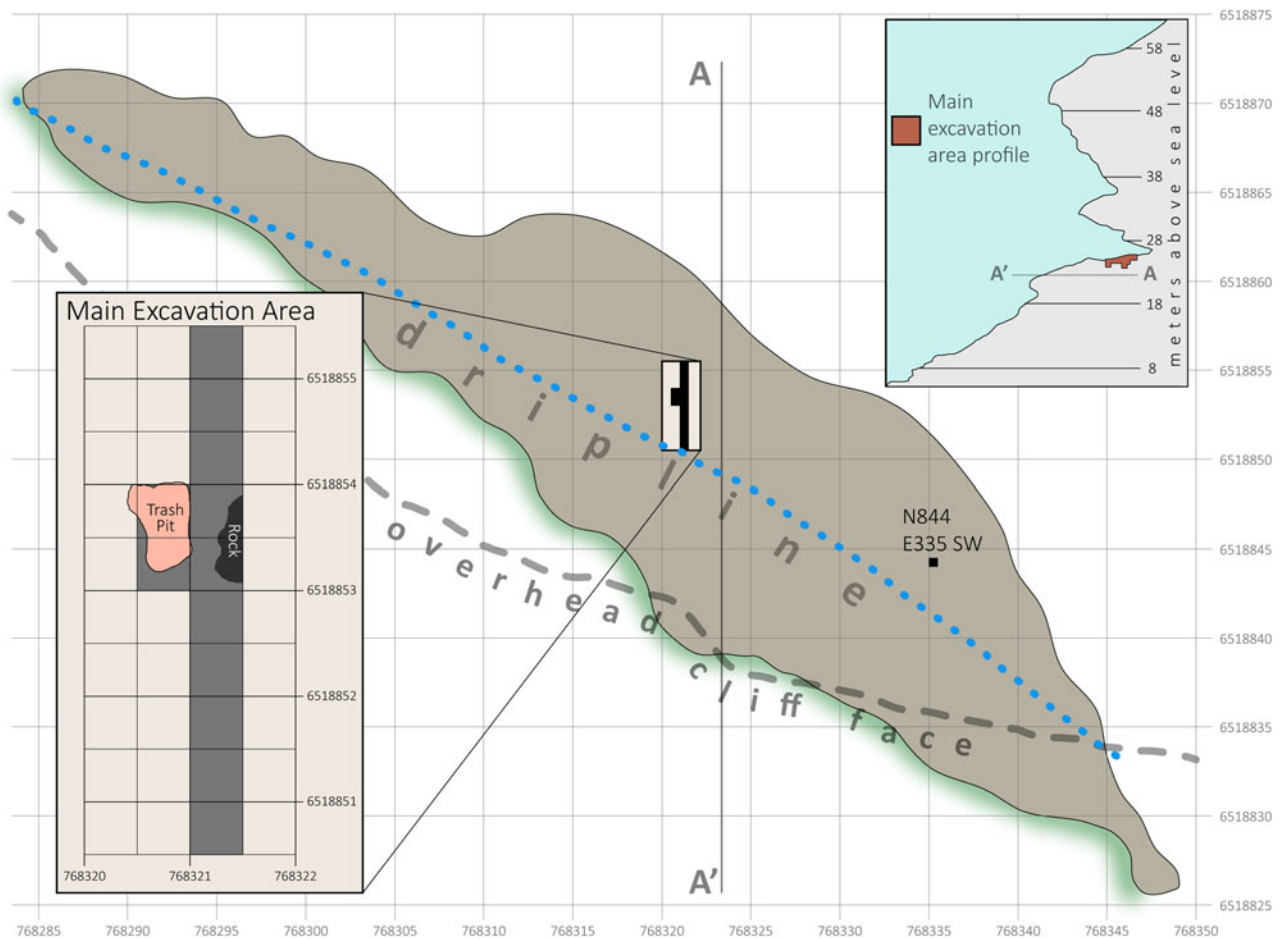
The Pondoland Paleoclimate, Paleoenvironment, Paleoecology, and Paleoanthropology Project (P5) is an interdisciplinary and international collaboration of researchers focused on understanding human adaptations to coastal environments. Early work in Pondoland by P5 focused on identifying and describing coastal archaeological records in rock shelters and open-air contexts. In 2011, P5 surveyed the Mkambati Game Reserve and the Msikaba and Lambasi areas of eastern

Pondoland, documenting 20 rock shelters and 5 open-air sites, most having abundant marine mollusk shells, stone tools, and terrestrial faunal remains. These surveys provided the first modern archaeological inventory of coastal occupations in Pondoland, spanning the Early Stone Age to historic European shipwrecks. Full details of the survey and sites are provided in Fisher and colleagues (2013).

In 2015, P5 conducted test excavations at four previously documented open-air and rock-shelter sites within the study area (Fisher, 2016). One of these sites is a large, dry coastal rock shelter (~80 m × 20 m) located ~25 meters above mean sea level (amsl). Originally designated using its grid coordinates as Site A2SE-1 (i.e., the first site recorded within the SE sub-quadrant of survey grid square A2), the site is now generally referred to as “Waterfall Bluff,” and that name is used here (see Fisher et al., 2013 for details about the survey grid). The test excavations at Waterfall Bluff revealed well-stratified archaeological deposits with abundant stone artifacts, shell, well-preserved bone, and macrobotanical remains. In 2016, P5 expanded the excavation at Waterfall Bluff to 4 m × 1 m (Fig. 3). These excavations revealed a well-preserved stratigraphic sequence that exhibits a north-south gradient of stratigraphic preservation from the dripline (poorer preservation) to more protected spaces of the shelter (better preservation) (Fig. 4). Continued excavations at Waterfall Bluff since 2018 have exposed a larger sample of lower deposits at the site confirming better preservation of stratigraphy further inside the rock shelter.

### WATERFALL BLUFF

At Waterfall Bluff, the Mlambomkulu River terminates in a waterfall ~60 m high debouching into the Indian Ocean (see Fig. 2). The rock shelter is adjacent to the waterfall, faces SE, and its floor is currently ~24 m amsl. Wave-cut ledges near sea level are comparable to geomorphic features along the cliff face, and we hypothesize that incision by previous high sea levels was responsible for the formation of the



**Figure 3.** (color online) Planimetric map of Waterfall Bluff. This image shows a map of the site and excavation areas as well as key geomorphic features like the dripline and overhead cliff face. An inset showing the main excavation area is also provided, as is a cross section of the cliff face and rock shelter at A–A'. UTM 35S northing and easting coordinates in meters are provided along the north (vertical) and east (horizontal) axes.

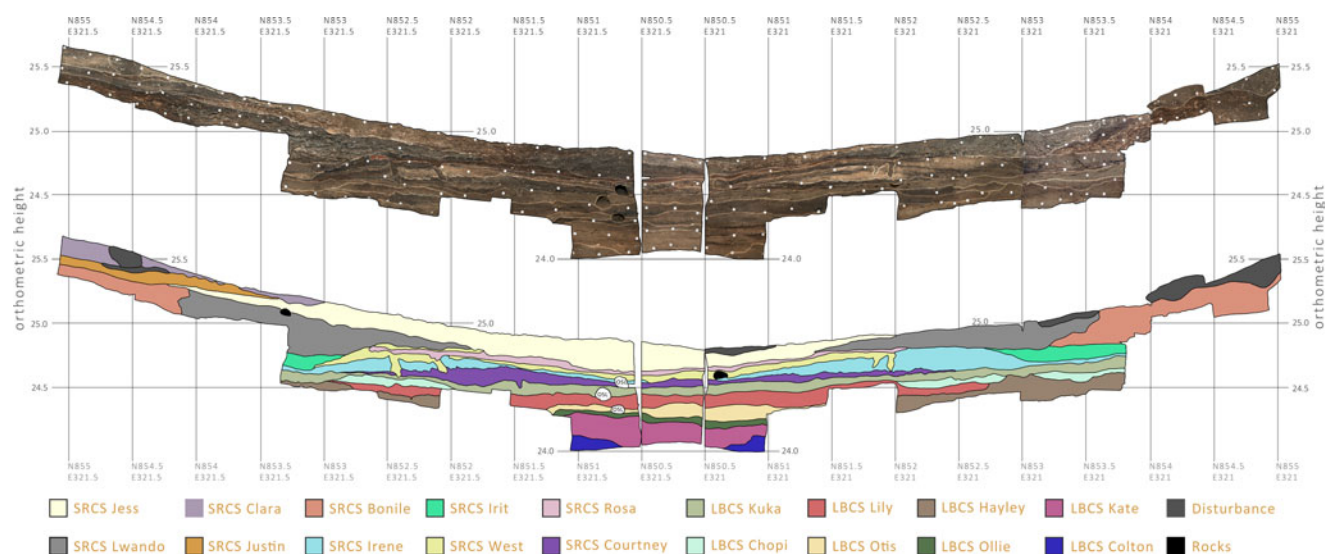
rock shelter during past high-sea stands. The rock-shelter incision has followed less-resistant layers of trough cross-bedded primary structures composed of moderately sorted quartz sand within the Msikaba Formation sandstones. More resistant beds of tabular quartz arenites appear to have contained the upper and lower boundaries of the incision, which is a pattern seen at other rock shelters across the region (Fisher et al., 2013).

Today, sedimentation within the rock shelter is low near the waterfall, and the bulk of archaeological deposits appear to be preserved within the main cavity of the shelter, >30 meters away. The modern surface of the rock shelter slopes  $\sim 10^\circ$  toward the mouth where there is erosion along the modern dripline. Just beyond the dripline, the surface plunges into a steep and jagged vegetated talus slope to the rocky coastline below. Supplementary File 1 provides a  $360^\circ$  interactive panorama of the site and the surrounding location with annotations describing the dripline and deposits.

The rock shelter is adjacent to a narrow continental shelf that limits the range of coastline changes. A composite gridded map of the regional bathymetry has been compiled from multiple existing datasets, providing a detailed look at

the seafloor surface around Waterfall Bluff (see Fig. 1). Data from the South African Navy hydrographic chart SAN 130 (Port St. Johns to Port Shepstone) were scanned, rectified, and digitized. Satellite altimetry data from the ETOPO1 1 arc-minute global relief model were also integrated into the model (Amante and Eakins, 2009). Single-beam echo-sounding data from the bathymetric map for southern Africa by Dingle and colleagues (1987) were also compiled, as were archival data stored on the South African Council for Geoscience Marine Geoscience server. In total, 41,277 data points were digitized covering a depth range from 0 to 500 m below msl. Interpolation of the error-corrected XYZ points (latitude, longitude, and depth) into the digital elevation model using a kriging technique was done using Golden Software Surfer 8.

The bathymetric data presented here from the adjacent seafloor cover a depth range of  $-500$  m to the shoreline. The data reveal a continuation of the sub-aerially exposed Pondoland coastal plain. Most broadly, outcropping of the Msikaba Formation sandstone on the inner- to mid-shelf has resulted in a lithologically influenced terrace that drops to the outer-shelf at an average depth of  $\sim 75$  m. Outcrops of the Msikaba Formation terminate in the south against the Egosa fault on the



**Figure 4.** The stratigraphic sequence from the main excavation area at Waterfall Bluff. This image shows the E321.5 profile (left), the N850.5 profile (center) and the E321 profile (right), which are adjacent and wrap around three-quarters of the main excavation area at Waterfall Bluff. At top is the color-corrected, high-resolution, georectified photomosaic of the sections that was created from >300 individual photographs. SubAggregate boundaries have been superimposed on this image, and the lower image shows the SubAggregates more clearly. A color key reference of the SubAggregates is provided below. The vertical axis represents orthometric height in meters, and the horizontal axis represents truncated UTM35S northing and easting coordinates. (For interpretation of the references to color in this figure legend, the reader is referred to the web version of this article.)

coastal plain (Johnson and Karpeta, 1979) and in the marine environment; this corresponds to the northern boundary of an embayment in Mbotyi that reflects this distinct lithological change. Bathymetric texture in this embayment on the seafloor is indicative of sedimentary accumulation, which stands in contrast to the dominantly sediment-starved, current-swept shelf to the north and adjacent to Waterfall Bluff. This sedimentary accumulation in the south has been described by Flemming (1981), who suggested deposition by a topographically controlled, northward-flowing, current gyre.

Mirroring the topography of the coastal plain, steep and deep paleoriver channels in the form of submarine canyons incise the continental shelf. These erosional canyons are oriented perpendicular to the present coastline and generally follow the offshore trajectories of modern rivers (see Fig. 1). Additionally, remnant deposits from Pleistocene sea-level changes are prevalent across the East Coast shoreline and continental shelf (Martin and Flemming, 1987; Cawthra et al., 2012; Bosman, 2013; Pretorius et al., 2019), and these rocks consist of aeolianite and cemented beach deposits. Scattered remnants of submerged paleocoastlines that lie parallel to the modern shoreline and are limited in lateral extent are preserved in the area under consideration at depths between 30 and 50 m below msl.

### Excavation methodology

The P5 excavation methodology is adapted from protocols developed by the South African Coast Paleoclimate, Paleoenvironment, Paleoecology, and Paleoanthropology (SACP4) project for 3D mapping and record keeping (Bernatchez

and Marean, 2011; Oestmo and Marean, 2014). In preparation for excavations, we established geodetic control at the site using a Topcon Hyper XT RTK Global Navigation Satellite System (GNSS) system to survey permanent control points in front of the rock shelter within the Universal Transverse Mercator (UTM) coordinate system (Zone 35S, World Geodetic System [WGS] 1984). GNSS static station measurements were recorded in 1-second intervals over 3 hours to account for ~100 km baseline lengths to the nearest TrigNet stations at Kokstad and Mthatha. Static station vectors were calculated to each TrigNet station using Carlson Survey GNSS 2016 software, and a least-squares adjustment was used to correct the rover data. Fixed L1 solutions with 100% ambiguity fixing was achieved for each point. The maximum 3D position of the mean dilution of precision (PDOP) was 2.2 with a mean PDOP of 1.8. Ellipsoidal WGS84 elevations were then converted to orthometric heights using SAGEOID10 (Chandler and Merry, 2010). We used these control points and a Topcon ES-105 reflectorless total station to traverse into the rock shelter and survey additional control points on the shelter walls. The control points inside the rock shelter now enable our total stations to be set up anywhere within the rock shelter and surrounding landscape and be tied into the global UTM system for precise and accurate digital measurements.

Using the UTM system, we have gridded Waterfall Bluff into 1-m squares where each square is named using the last three digits of the UTM Easting and Northing coordinate of the southwest (SW) corner of the square. Furthermore, excavations are conducted within 50 cm × 50 cm quadrants within each square, designated as SW, northwest (NW), northeast

(NE), or SE. Therefore, N854E321SE refers to the SE quadrant within grid square N854E321, itself having SW corner coordinates Northing 6518854.0 and Easting 768321.0.

All excavations follow natural stratigraphy, and our tiered classification of the stratigraphy follows the methodology of Karkanas and colleagues (2015). Accordingly, stratigraphic layers (i.e., “StratUnits”) represent anthropogenic and geogenic changes in sediments that are visible during excavations. StratUnits are grouped into larger “SubAggregates” (i.e., “SubAggs”), which represent identifiable and discrete anthropogenic, biogenic, or geologic events. A cluster of shell-rich deposits with interdigitated fine sterile layers, for example, may be classified as a SubAgg if it can be shown that these layers were deposited contemporaneously and under similar processes. SubAggs are then consolidated into “Stratigraphic Aggregates” (i.e., “StratAggs”), that are laterally continuous sediments across large areas. These sediment groups represent periods of specific formation processes throughout a site’s life history. StratUnits are identified using an alphanumeric system. StratUnit WB16AC, for example, refers to the 29<sup>th</sup> StratUnit assigned at Waterfall Bluff during the 2016 field season (i.e., 26 StratUnits from A to Z, then cycling to AA, AB, AC, etc. for StratUnits 27 and so on). SubAggs are assigned proper names associated with the project. StratAggs are identified using an acronym indicating the broad characteristic of the sedimentological group, like SRCS, which means “Shell-Rich Clayey Sands.” Throughout this paper, we refer to all deposits and archaeological materials with reference to StratAggs and SubAggs, descriptions of which are provided in Table 1 and Figure 4.

Additionally, each StratUnit is assigned a unique “Lot Number,” which is a bulk tracking number. It is assigned to all artifacts, fauna, or features that are mapped and/or collected within a single quadrant of a single StratUnit. All 3D-plotted archaeological materials and fauna are further assigned unique Catalog Numbers (CN). References to specific artifacts or samples always include the Lot and CNs (e.g., CN123456, Lot 123), which identify the unique ID of every object but also constitute a direct link to full contextual information about the object’s provenience in our Microsoft Access tabular records and in our 2D and 3D Geographic Information System databases.

All sediments removed during excavations are wet-sieved through nested 5-mm, 3-mm, and 1.5-mm screens before the remainder is dried and bagged individually using the Lot Number, StratUnit, and mesh size to identify the bag’s provenience and contents. In the P5 laboratory at the East London Museum, these screened materials are sorted into different categories (e.g., shell, stone, fauna, etc.), and all identified screened materials are assigned their own CNs and placed into individual plastic bags.

Except for during our earliest test excavations, we plot all archaeological remains (including, but not limited to artifacts, charcoal, ochre, macro-plants, terrestrial and marine fauna, and shellfish) and samples for specialized analyses (e.g., geochronology, geochemistry, palynology, phytoliths, plant wax isotopes, and magnetic susceptibility) in 3D with a total

station. We also collect sediment samples from each StratUnit—known as a “Bulk Sample”—for any additional analyses that might be found useful in the future. Every rock >5 cm found during excavations is also mapped, as is every StratUnit surface. At the end of excavations, we use a Nikon D300s and 35 mm f1.8 lens to create high resolution (~1 mm pixel resolution), color-corrected photomosaics of all stratigraphic profiles that are georectified in 3D. These methods are described in Fisher and colleagues (2015), except that Imatest 5.1 is now used to color correct the imagery.

The site and surrounding cliffs have been mapped using a combination of total stations (Topcon ES-Series and North-west NTS02S), RTK GNSS (Topcon Hyper XT and Carlson BrX5), and forward-facing georectified parallax photography via a DJI Mavic 2 Pro and a Phantom 2 mounted with a GoPro Hero 3+. These data, and the excavated point-plot data, have all been integrated into a high-resolution and photorealistic 3D Geographic Information Systems model using ArcGIS Pro 2.1.3, and to a lesser extent ESRI ArcGIS 10.6. The models allow our team to make detailed observations about the rock shelter, excavated archaeological deposits, cliffs, and surrounding coastal shelf to understand site formation processes and, ultimately, the context of the archaeological deposits.

## Excavation history

Excavations began at Waterfall Bluff in 2015 with the excavation of two 50-x-50-cm test pits. One test pit (N844E335SW) was located in the southeastern part of the rock shelter whereas the other (N854E321NW) was located near the central/NW part of the rock shelter. Both excavations were located within the dripline and on the gently sloping surface that backs up against the rear of the site.


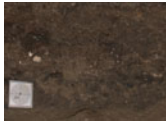




Quad N844E335SW reached a maximum depth of ~60 cm. Excavations here ended prematurely on account of time, but they revealed a well-stratified archaeological sequence. Observations of the east- and west-facing profiles within quad N844E335SW suggest that the contemporary 10° slope of the rock shelter surface may be due to erosion of deposits underlying modern overburden sediments (Fig. 5).

Quad N854E321NW, in the center of the shelter, reached a maximum depth of ~45 cm before reaching a large, flat stone surface that we now know to be a fallen block from the roof. In 2016, we expanded the excavations around quad N854E321NW and were able to excavate around the roof block and remove it, revealing more archaeological deposits underneath. The excavation area was also expanded laterally to 4.5 meters long x 0.5 meters wide on a north–south axis (see Fig. 4). The location of the 4.5-m-long trench was designed to intersect the dripline at the south end of the excavations (i.e., along the N850.5 line) and provide information on sedimentological and archaeological preservation in the shelter.

The deepest current excavation areas at Waterfall Bluff are located at the dripline in quad N850E321NW (see Fig. 4). Here, we excavated to ~80 cm below the modern shelter surface. These excavations revealed stratified archaeological







**Table 1:** Table summarizing the SubAggregate stratigraphy at Waterfall Bluff. This table provides details about the stratigraphy at Waterfall Bluff in chrono-stratigraphic order whenever possible. Black bars are used to represent non-contiguous contacts for spatially isolated layers within the overall chrono-stratigraphic sequence. The 68.2% modeled radiocarbon boundary ages (see Table 2) and 1-sigma optically stimulated luminescence (OSL) results (Table 3) for SubAggs are provided as a reference when available.

Strat. Agg.	SubAgg.	Modeled age, from (cal yr BP)	Modeled age, to (cal yr BP)	Munsell color	Sedimentological description	Archaeological Description	Interpretation		
<b>N844E335SW</b>	<b>SRCS</b>		Unmodeled <sup>14</sup> C 8,288 - 8,025	7.5YR 5/3 brown	Loosely consolidated dark, organic-rich sand.	Stone artifacts, bone, and charcoal are present. Shell preservation is variable, and many shells appear crushed.	SubAgg has undergone more weathering compared to other SRCS shell-rich units like SRCS Lwando or SRCS Bonile.		
	Josh - Nate Contact								
	Josh		Unmodeled <sup>14</sup> C 8,395 - 8,203	10YR 2/1 black	Loosely consolidated shell-rich sand.	Stone artifacts, bone, and shell; however, bone—particularly burnt bone—is especially common. Charcoal is also present.			
<b>SRCS</b>	Justin	10,750 - 10,720	10,740 - 10,670	10YR 2/1 black	Mottled ash and charcoal-rich sandy clay.	Shell is common, but stone artifacts are infrequent. Small shell fragments and burnt bone are common.			
	Bonile - Justin contact					Gradational contact.			
	Jess	10,770 - 10,730	10,750 - 10,720	7.5YR 4/2 brown	Dense lenticular layer of well-preserved Perna perna shells in a shell-supported matrix lending a golden coloration. There is very little sediment within the SubAgg. Toward the dripline shell becomes less frequent to rare and the coloration of the sediments darkens considerably.	Bone is common and well preserved, including bone tools and stone artifacts. Shell is less frequent toward the dripline.	Shell midden that has been decalcified by dripwater under the dripline.		
	Lwando - Jess contact								
	Lwando	10,790 - 10,740	10,770 - 10,730	10YR 3/1 very dark gray	Loosely consolidated grey shell-supported matrix dominated by burnt Perna perna shells that lend a characteristic grayish color. Sediments surrounding the shells are poorly sorted medium sands.	Preserved macrobotanical remains, including leaves and seeds, are present. Bone and charcoal are also common. Stone artifacts are present, though in lower quantities.	The presence of preserved macrobotanical remains and low amounts of charcoal and ash suggest the shells are in secondary context.		
	Rosa - Jess Lwando contacts								
	Rosa	No radiocarbon ages.	No radiocarbon ages.	7.5R 2.5/3 very dusky red	Banded dark red sand. The sand extends from the dripline of the rock shelter nearly the entire length of the 4.5-m trench, pinching out by N854, but creating a distinctive marker horizon. There are isolated pockets of ash and sand within SRCS Rosa.	Stratified shell, stone artifacts, and bone are relatively more common.	Currently believed to be a slab of ochre that was either intentionally disturbed or naturally eroded across the shelter floor before being buried.		
	West - Rosa / Lwando / Irit contacts								
	West								



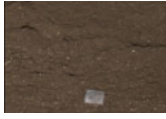

(Continued)

**Table 1:** Continued.

Strat. Agg.	SubAgg.	Modeled age, from (cal yr BP)	Modeled age, to (cal yr BP)	Munsell color	Sedimentological description	Archaeological Description	Interpretation	
		No radiocarbon ages.	No radiocarbon ages.	2.5YR 3/2 dark olive gray	Ash-rich sediments with several well-preserved combustion features. Around N852, there are numerous vertical infilled incisions ~20 cm in diameter. The incisions all start in SRCS West and crosscut SRCS Irene and SRCS Courtney. There is evidence to suggest some of the incisions are spatially aligned.	Stone artifacts and bone are found throughout SRCS West, but become less frequent toward its base.	The incisions are currently hypothesized to represent post holes of unknown function.	
<b>SRCS</b>								
	Bonile - Lwando contact							
	Bonile	11,040 - 10,750	10,790 - 10,740		Thick, reddish-brown, loosely consolidated silty-sand. SRCS Bonile has a very light texture on account of high organic content that includes well-preserved macrobotanical remains, which are often found adhering to the undersides of mussel shells. SRCS Bonile has been truncated around N854 in antiquity and is likely coeval with deposition.	Charcoal is common within SRCS Bonile, as are well-preserved bone, bone tools, stone artifacts, and shell beads.	SRCS Bonile was partly dug to make room for the deposition of the SRCS Lwando shells.	
	Irit - Bonile / Lwando contacts							
	Irit	11,050 - 10,970	11,040 - 10,750	5YR 4/3 reddish brown	Medium/fine reddish-brown sand.	Terrestrial animal bone, abundant marine fish bone and marine shellfish, and stone artifacts are present.		
	Irene - Irit / Lwando / West contacts							
	Irene	11,060 - 10,990	11,050 - 10,970	10YR 2/1 black	Thin, dark band of organic-rich sand and charcoal that is similar in character to SRCS Bonile despite differences in color. Matrix-supported deposits composed of coarse-grained archaeological material in a fine-to medium-sand grained matrix. The grain size distribution is bimodal, and quartz clasts are discoidal to spherical. Shell fragments are generally tabular and irregular. SRCS Irene is poorly sorted as a whole, with a moderately well-sorted matrix. Shell layers and coarse clasts associated with these are imbricated and the combustion features are wavy, but the beds above and below are tabular and continuous.	Stone artifacts are infrequent, but bone is visibly better preserved than in other SRCS SubAggs; 0.5 – ~1 cm-diameter water-worn stones were also relatively more common. The coarse-grained archaeological materials are composed of shell fragments and charcoal, and the matrix material is made up of ash and suspected burnt turf.		
	Courtney - Irene				Sharp contact.			

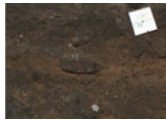


(Continued)

**Table 1:** Continued.

Strat. Agg.	SubAgg.	Modeled age, from (cal yr BP)	Modeled age, to (cal yr BP)	Munsell color	Sedimentological description	Archaeological Description	Interpretation	
	Courtney	11,160 - 11,050	11,060 - 10,990	2.5YR 2.5/5 dark reddish brown	Dark, moist, clay-sand with abundant charcoal. SRCS Courtney contains large quartz clasts and burnt bone. The dominant grain size is coarse sand, and the grain shapes vary according to composition. Charcoal fragments are tabular to irregular, soil fragments are equant to irregular, shell fragments are tabular, and quartz clasts are generally sub-rounded to angular. Quartzite roof spall is spherical to equant. As a whole, SRCS Courtney is very poorly sorted, and three sedimentary sub-units are vaguely separated by combustion features. Grain size is normal graded, and bedding is parallel- to sub-parallel. Secondary structures and features include large voids, making this unit porous and permeable.	Abundant shellfish, marine fish bone, terrestrial animal bone, and stone artifacts. Surrounding the burnt bone is a black halo of unknown composition. Rubified combustion features and ash layers characterize this SubAgg, as well as intermittent clumps of soil, suspected to be burnt. Charcoal and limited shell fragments are present, but these are less abundant than in Irene.	Cross-stratified combustion features.	
		OSL 13.3 ± 0.7 ka						
	SRCS - LBCS contact				Sharp contact, but does not appear to be erosional.			
LBCS	Kuka	13,880 - 13,510	13,470 - 13,130	10YR 4/3 olive brown	Coarse, loosely compacted sand with sub-rounded grains and 1-2 cm roof spall. LBCS Kuka contains a relatively high percentage of roof spall, within a matrix of clay. As a whole, this unit is a clast-supported conglomerate. The dominant grain size is medium sand, and the grain shapes are tabular (charcoal) and spherical to equant (quartzite). The deposits are poorly sorted and have subtle layering. Bedding laminae are discontinuous in form at the top of the unit and curved and wavy-parallel near the base.	Terrestrial animal bone, marine fish bone, and stone artifacts are present. Rubified combustion features contain ash layers, charcoal, bassanite (?), and soil aggregates.		
		OSL 12.5 ± 1.2 ka						
N844E335SW LBCS	Siyambonga	No radiocarbon ages.	No radiocarbon ages.	10YR 4/6 olive brown	Coarse, compacted sands with sub-angular grains and <1 cm roofspall.	Terrestrial animal bone, charcoal, and stone artifacts.		
LBCS	Chopi-Kuka contact				Irregular and jagged.			
	Chopi	18,080 - 17,260	15,050 - 14,380	5YR 4/4 reddish brown	Loosely compacted, coarse, dark brown sand with 1-2 cm, irregular, sub-rounded roofspall containing inter-stratified layers of charcoal and ash.	Terrestrial animal bone, marine fish bone, marine shellfish, charcoal, and stone artifacts.	Repetitive occupation and construction of combustion features.	
	Kuka-Lily contact				Sharp and distinctive contact with a curved but not undulatory morphology.			




(Continued)

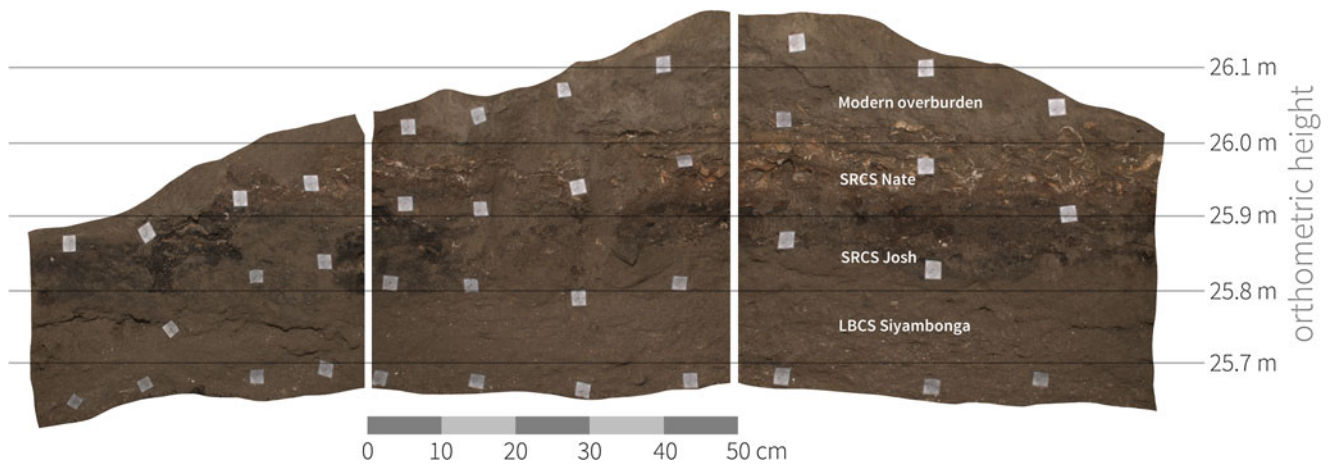
Table 1: Continued.

Strat. Agg.	SubAgg.	Modeled age, from (cal yr BP)	Modeled age, to (cal yr BP)	Munsell color	Sedimentological description	Archaeological Description	Interpretation	
LBCS	Lily	22,560 - 21,900	20,190 - 19,340	7.5YR 3/2 dark brown	Coarse sand with sub-rounded grains and 1-2 cm roofspall. Charcoal is common, as are ash and chunks of bassanite. The grain shape of quartzite is angular to sub-angular quartzite, and quartz is spherical to equant. Charcoal is cylindrical and tabular. This unit is very poorly sorted and contains no clear bedding structures. It is largely unstratified.	Terrestrial animal bone and stone artifacts. Ash layers and charcoal increase near the base.	Cross-stratified combustion features	
	Otis-Lily contact				Gradational. Uppermost LBCS Otis sediments have been thermally altered. Distinct color changes above and below help to differentiate the location of the contact.		Continuous deposition.	
	Otis	23,080 - 22,600	22,560 - 21,900	7.5YR 3/2 black	Light gray, loosely compacted, sub-angular, coarse-grained sands. <1 cm roofspall inclusions. Grain sizes are larger overall compared to underlying LBCS Otis, Kate, or Colton. LBCS Otis is composed of quartz, feldspar, rubified combustion features, burnt remains, and bone fragments. The geogenic clasts are generally spherical to equant, and the unit is characterized by alternating beds of coarser and finer grain size. Layered combustion features are interbedded with seemingly archaeologically sterile layers. These beds are tabular and blocky and vaguely parallel. Secondary features include voids.	Low density of archaeological remains.	Period of continuous sedimentation with low-occupation.	
	Otis-Ollie contact		OSL 22.1 ± 1.3 ka		Gradational. LBCS Otis sediments are finely intermixed with larger particles of charcoal and white residue (bassanite?) from uppermost LBCS Ollie. Difficult to distinguish this contact in thin section.		Continuous deposition.	
	Ollie	No radiocarbon ages.	No radiocarbon ages.	7.5YR 2/2 very dark brown	Dark, charcoal-rich layer with poorly sorted, angular grains and <1 cm angular roofspall. This poorly sorted unit is made up of roof spall, quartz, and significant combustion features. Burnt clumps of soil and charcoal are present.	Lithics, charcoal, terrestrial animal bone, marine fish bones, and shellfish fragments.	Cross-stratified combustion features.	
	Kate-Ollie contact				Gradational.		Continuous deposition.	

(Continued)

Table 1: Continued.

Strat. Agg.	SubAgg.	Modeled age, from (cal yr BP)	Modeled age, to (cal yr BP)	Munsell color	Sedimentological description	Archaeological Description	Interpretation	
	Hayley	28,100 - 27,150	24,050 - 23,160	10YR 6/4 light yellowish brown	Loosely compacted, coarse sand with <1 cm angular roofspall. Throughout the SubAgg are thin lenses of either charcoal- or ash-rich sediments overlying rubified sediments. Many of the charcoal- and ash-rich lenses have been truncated by other charcoal-rich sediments.	Stone artifacts, terrestrial animal bone, charcoal, and marine shellfish.	Combustion feature maintenance and construction from repeated human occupation.	
	Kate	32,000 - 31,100	31,000 - 30,100	2.5YR 4/4 reddish brown	Moist, loosely compacted, coarse sand with <1 cm angular roofspall. The coloration of these sediments is distinctly redder than LBCS Colton. There are also multiple, discrete lenses of charcoal-rich sediments overlying rubified sediments. Flecks of bassanite are also present. LBCS Kate is composed of quartz clasts in a matrix containing clay minerals. Bassanite occurs in the sedimentary layers, as well as small fragments of charcoal. This SubAgg is poorly sorted. This unit is finer grained than the layers above and has no clear bedding structure. Quartz and rock fragments of quartzite are spherical, irregular, and equant. Bassanite is tabular and irregular.	Stone artifacts, terrestrial animal bone, marine shell, and charcoal.	Intermittent combustion feature construction interspersed with periods of human non-occupation of unknown duration.	
	Colton-Kate contact		OSL 27.8 ± 2.1 ka		Gradational contact that is difficult to discern. This surface dips at an angle of up to 45°.	Continuous deposition.		
	Colton	No radiocarbon ages.	No radiocarbon ages.	10YR 5/4 light olive brown	Moist, loosely compacted, coarse sand with <1 cm angular roofspall. The sand grains are sub-rounded and poorly sorted. There are distinct flecks and bands of white residue throughout the sediments. X-ray diffraction (XRD) and scanning electron microscopy (SEM) analysis of the white residue confirms that it is bassanite, CaSO <sub>4</sub> ·0.5(H <sub>2</sub> O), which is related to gypsum. Overall, Colton has a grayer coloration compared to overlying LBCS Kate. Alteration rims of clay minerals are noticeable at grain boundaries. The deposit is poorly sorted. Quartz is spherical to equant; bassanite is tabular.	Terrestrial animal bone and stone artifacts, as well as small pieces of charcoal and fragments of marine shell.		
			OSL 37.6 ± 4.2 ka					



**Figure 5.** (color online) Stratigraphic profiles from quad N844E335SW. Quad N844E335SW is located in the southeast section of the rock shelter at Waterfall Bluff. The sequence shows a coarse sandy layer (Light Brown Coarse Sands [LBCS] Siyambonga) that is similar to other LBCS sediments elsewhere on site. Above this, the sedimentology is more clayey and reminiscent of the Shell-Rich Clayey Sands (SRCS). Two SRCS SubAggregates have been identified, charcoal-rich SRCS Josh and shell-rich SRCS Nate.

layers and a major change in sediments representing two distinct StratAggs, which are described below. Bedrock has not yet been reached.

During the course of excavations, we uncovered a recent trash pit, ~80 cm wide  $\times$  ~50 cm deep, that had been dug into archaeological deposits between N853 and N854 and that was partially burned *in situ* (see Fig. 3). Using a Cadbury Smash instant mashed potato wrapper found within the deposit, we were able to relatively date the trash pit to the mid–late 1970s. We opted to excavate the trash pit *en masse*, which exposed an ~1-m-wide pit that we continued to excavate to expose underlying *in situ* archaeological deposits.

In 2019, significant efforts were made to deepen the main excavation trench to collect a larger sample of archaeological materials from SRCS and Light Brown Coarse Sands (LBCS) contexts and to provide more information about the stratigraphy. These excavations have revealed a complex stratigraphic sequence, which shows evidence for not only vertical accretion of deposits, but also lateral accretion from the rear of the rock shelter toward the mouth. Stratigraphic preservation does, therefore, appear to increase within the confines of the shelter, and many SubAggs can now be traced across most of the excavated trench (see Fig. 4).

### Stratigraphic sequence

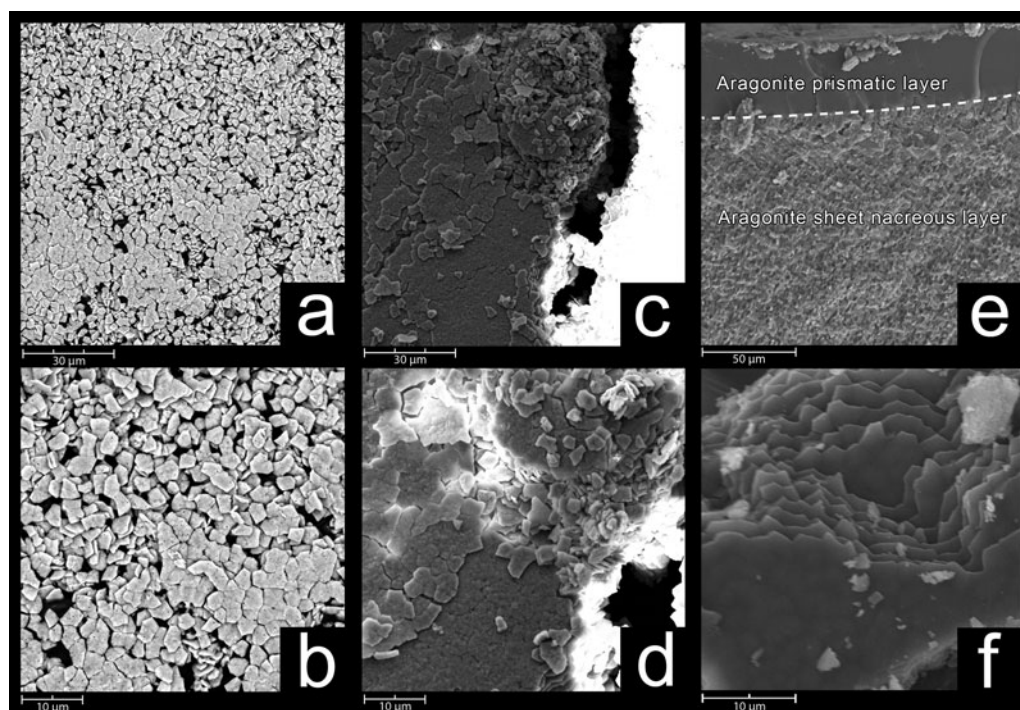
We have subdivided the current excavated deposits into two StratAggs, named the LBCS and the SRCS. Currently, the deepest StratAgg is the LBCS. Figure 4 shows the primary stratigraphic profiles at the site as well as the locations of each SubAgg documented to date. Additionally, Table 1 summarizes the sedimentology and archaeology of each SubAgg and provides comments regarding how these layers are currently interpreted. A detailed micromorphological investigation is under way.

In general, the LBCS is characterized by loosely compacted moist coarse sands. Interspersed within these sands are darker

deposits having relatively greater archaeological remains, ash, and charcoal. None of the deposits completely lack archaeological remains. This suggests that the site was never abandoned for prolonged periods of time during the LGM like sites in the surrounding highland and inland areas (Stewart and Mitchell, 2018). Instead, the changes in archaeological content across the LBCS may signal fluctuations in occupation intensity or differential use of the site over time, though aspects of duration or periodicity are currently unknown.

Multi-proxy evidence of marine shellfish and marine fish remains have now been recovered from multiple LBCS layers attesting to the proximity of the coastline during this time. At the dripline, this evidence ranges from microscopic to macroscopic. For example, scanning electron microscopy (SEM) and X-ray diffraction (XRD) have been used to identify microscopic traces of dissolved shellfish in LBCS Kuka representing mytilid mussel (probably the locally dominant *Perna. perna*) based on the microstructure of the shell (Fig. 6). Subsequent investigations have also revealed marine shell fragments and marine fish bone, which are relatively better preserved from LBCS layers found inside the rock shelter, though most of these materials remain under investigation and are not reported here.

Stratified above the LBCS, the SRCS is sedimentologically distinct, having a dark, clay-rich composition nearly lacking in roof spall. The SRCS stratigraphy is complex, and there are several instances where SRCS deposits have been truncated and modified by prehistoric site inhabitants contemporaneously with their formation. One of the clearest examples of this kind of site modification is found in SRCS Bonile, which was truncated between N853.5 and N854 soon after deposition to make room for the deposition of the SRCS Lwando midden (see Fig. 4). SRCS Lwando itself is composed of predominantly burnt shells, yet there is little evidence of *in situ* combustion features, which suggests the Lwando shells are in a secondary context and were dumped in the hole created from the removal of SRCS Bonile after they had been burned.



**Figure 6.** Scanning electron microscopy (SEM) of shellfish. SEM nacre tablets present in sediment sample 315 Kuka (a–d). Images (c) and (d) show the nacre tablets formed as sheets, which match with the modern mussel (*P. perna*) samples (e, f) that highlight the interior aragonitic sheet nacreous microstructural layer. SEM images were taken with various settings due to a high occurrence of beam charging—seen in images (c) and (d)—despite sputter coatings of carbon and gold. (a) and (b) 10Kv backscatter electron detector. (c) and (d) 10kv secondary electron detector (SED). (e) 15Kv SED. (f) 20Kv SED.

The same sequence of StratAggs is also seen in N844E335SW (see Fig. 5). The test excavation is ~15 meters SW of the main trench. The current lowest deposit is an undated roofspall-rich coarse-grain sand called LBCS Siyambonga. This deposit is overlain by loosely consolidated dark and organic-rich sands, which have been subdivided into two SubAggs, SRCS Josh (lower) and SRCS Nate (upper).

## CHRONOLOGY

In this study, we have used a combined AMS radiocarbon ( $^{14}\text{C}$ ) and single-grain OSL dating approach. AMS radiocarbon dating was used to establish a chronology of anthropogenic materials found in the archaeological excavations, and OSL dating was used to establish a chronology for the sedimentary sequence exposed through excavation. The methods are complementary and provide unique insights into the depositional history (OSL) and archaeological occupations (AMS radiocarbon) at the site. The results can also be used to independently test the chronologies to identify factors that may be influencing results.

### Chronology Methods

#### AMS $^{14}\text{C}$ Dating Methods

Fifty-one AMS  $^{14}\text{C}$  samples have been dated from our catalog of piece-plotted wood charcoal. The proveniences of all

samples are listed in Supplementary File 2. Charcoal wood identification of the samples is currently under way. Most of the charcoal was piece-plotted *in situ* and put into individual sterile plastic containers immediately upon discovery to limit contamination.

The initial radiocarbon analysis was conducted by Beta Analytic, Inc, and these samples are reported in Supplementary File 3. Using an acid-alkali-acid pretreatment procedure, these samples were first floated and agitated in deionized  $\text{H}_2\text{O}$  to disperse the sediment. They were then progressively sieved through 250- and 180- $\mu\text{m}$ -diameter sieves to remove any plant macrofossils or rootlet material prior to pretreatment. The <180  $\mu\text{m}$  fraction was then subjected to a series of hot (near boiling) 0.5N HCl leaches to remove any carbonates before being immersed in an alkali wash (NaOH), which removed secondary organic acids. The samples were then rinsed with deionized  $\text{H}_2\text{O}$  until neutral and dried in a 70°C oven overnight. The pretreated sample material was then homogenized and examined under a 45 $\times$  microscope to inspect for any rootlet hairs or fragments. A portion of each sample was tested with 0.5N HCl again to ensure that all carbonate had been removed. The sample was then combusted to  $\text{CO}_2$  and graphitized for AMS counting.

P5 has subsequently partnered with iThemba Laboratory for Accelerator Based Sciences (iThemba LABS) to promote their AMS dating facility, which is currently the only one operating in Africa. Charcoal sub-samples measured at iThemba LABS were pre-treated with a standard

acid-base-acid treatment: 1% HCl, 1% NaOH, and 1% HCl, respectively. Each treatment step was carried out for 45 minutes at 70°C. Sub-aliquots of the pre-treated sample were analyzed for  $\delta^{13}\text{C}$  at the stable isotope facility of the University of Pretoria.

For  $^{14}\text{C}$  analysis, the pre-treated charcoal samples were graphitized at the iThemba LABS graphitization line and then pressed as sputter target for AMS analysis. The AMS system at iThemba LABS is based on a 6MV EN tandem multi-sample Cs-sputter ion source (similar to the models used by Lawrence Livermore National Laboratory and Prime-LAB), a multi-beam switching system capable of fast cycling between isotopes (run at 5 cycles per second), and a modern AMS analysis beam-line supplied by NEC (Mbele et al., 2017). At the accelerator we use  $^{13}\text{C}$  for normalization, and  $\delta^{13}\text{C}$  correction is based on the conventional mass spectrometry measurements. Samples were normalized and blank corrected against graphitized samples of the OXII standard and our fossil coal blank material (the latter pre-treated with the same protocol as the charcoal), respectively. In a measurement run, up to 43 unknown samples are analyzed together with a set of at least 5 OXII standard samples for normalization. In addition, 6 blanks are routinely measured in every such run; however, a long-term averaged blank value and the corresponding long-term standard deviation is used for the correction. The samples in the ion source cycled through several times to check against possible long-term drifts. Together with fast-cycling and the use of “bad-cycle” rejection, we can thus eliminate both short-term and long-term conditions not conducive to high reproducibility. AMS data analysis follows the concepts put down by Puchegger and colleagues (2000).

Additionally, a previous set of charcoal samples that were measured by Beta Analytic, Inc. and that still had material available was subsequently measured at iThemba LABS. The results between the laboratories for these samples agree within error. A set of samples have also been run in duplicate at iThemba LABS to affirm overall sample pre-treatment and AMS inter-run reproducibility. The individual AMS radiocarbon results for iThemba LABS measurements and combined values for the charcoal samples are available in Supplementary File 3.

The Bayesian radiocarbon age model presented herein is based on 51 radiocarbon dates of charcoal samples for 13 SubAggs, using OxCal v4.3 (Ramsey, 2009a). SHCal13 (Hogg et al., 2016) was used for calibration. The model parameters are provided in Supplementary File 4. The raw data from the model are provided in Table 2. The ages that are used here to describe each SubAgg, including in Table 1, are based on data at the 68.2% confidence interval rounded to nearest decade between 10,000 and 25,000 BP; ages greater than 25,000 BP are rounded to the nearest half-century. This rounding prevents over-reporting of significant digits while ensuring that any shift thereby introduced stays below a sixth of the 68.2% range so as to be irrelevant. Lastly, Figure 7 provides a graphic illustration of the posterior density function and range and the unmodeled probability

density function and range for each sample and SubAgg boundary at the 68.2% range.

Based on the species analysis for the charcoal (ongoing and not presented here) we anticipate no significant old-wood effect. The SubAggs LBCS Kate and LBCS Hayley are modeled as potentially overlapping, and currently we do not have a radiocarbon date for LBCS Colton. The current excavated limits of LBCS Hayley do not overlap with LBCS Otis; therefore, it cannot provide a constraint on LBCS Otis or vice versa (see Fig. 4).

We have a sequence of deposition from LBCS Otis to SRCS Justin. The choice of contiguous boundary conditions from SRCS Courtney through to SRCS Justin is partly informed by the fact that any attempt to make them sequential (potentially allowing for a gap of deposition) does not yield any clearly evident gaps in deposition—all of them are consistent with 0 on both the 95.4% and 68.2% confidence intervals and are certainly below the resolution of radiocarbon measurements themselves. The sequential or contiguous boundary conditions elsewhere are informed by the evidence from the interfaces between the SubAggs. Specifically, we assume sequential boundary conditions between SRCS Courtney–LBCS Kuka, LBCS Kuka–LBCS Chopi, and LBCS Chopi–LBCS Lily, but contiguous boundary conditions between LBCS Lily and LBCS Otis. Of all the potential gaps in this specific sequence, only the one between LBCS Chopi and LBCS Lily could be considered substantially evident, but there is evidence to suggest this may be due to sampling strategy.

Modelling of the SubAggs within SRCS also proved problematic as the calibration curve intersects 3 times over a 500-year period for all SRCS results. Potentially small deviations, therefore, could have significant consequences around that time period and tip the whole set of SubAggs to the older or younger side of the wiggle. Four samples from this period show low agreement for the model; however, removing them did not have a significant impact on the modelling result, and they are therefore included. Furthermore, OxCal runs using a simple outlier model (Ramsey, 2009b) also did not conclusively suggest elimination. Thus, there is good indication that SRCS Courtney is on the older side while SRCS Lwando, Jess, and Justin are highly likely to be on the younger side, but the exact transition from SRCS Lwando to SRCS Courtney is highly uncertain and made difficult by SRCS Bonile having only one radiocarbon result.

### OSL Dating Methods

OSL dating provides an estimate of the amount of time elapsed since mineral grains were last exposed to sufficient sunlight (Huntley et al., 1985; Aitken, 1998; Duller, 2004; Wintle, 2014; Roberts et al., 2015). This method can be used to determine the depositional age of sediments and, by association, the age of material remains at archaeological sites. Four sediment samples were collected from the LBCS deposits, and one was collected from the transition between LBCS and SRCS. Sand-sized quartz grains were extracted



**Table 2.** AMS 14C Bayesian Analysis Results. This table provides the unmodeled and modeled results of a Markov Chain Monte Carlo analysis of the radiocarbon data from Waterfall Bluff at both 68.2% and 95.4% ranges. The SHCAL13 calibration curve (Hogg et al., 2016) was used. Results >25,000 BP were rounded to the nearest 50 years, and results between 10,000 and 25,000 years were rounded to the nearest 10 years to prevent over-reporting of significant digits.

Name	Unmodeled (cal yr BP)						Modeled (cal yr BP)						Indices Amodel 54.1 Aoverall 54.1				
	From	To	%	From	To	%	From	To	%	From	To	%	Acomb	A	L	P	C
Difference duration of SRCS							331	490	68.2	127	774	95.4					99.6
Difference duration of SRCS							-2	236	68.2	-2	253	95.4					95.4
Boundary end of Justin							10,740	10,670	68.2	10,770	10,500	95.4					99.8
Interval duration of Justin									59		240	95.4					99.9
Span of dates of Bonile-Justin									16		48	95.4					100
CN 6666	11,060	10,700	68.1	11,070	10,660	95.4	10,740	10,700	68.2	10,760	10,670	95.4		129.7			99.9
CN 1503	11,060	10,710	68.2	11,070	10,680	95.4	10,740	10,710	68.2	10,760	10,680	95.4		119.9			99.9
Phase Justin																	
Boundary end of Jess							10,750	10,720	68.2	10,770	10,700	95.4					99.8
Interval duration of Jess									20		50	95.4					100
Span of dates of Jess									14		36	95.4					100
CN 4945	11,100	10,790	68.2	11,130	10,760	95.4	10,760	10,730	68.2	10,780	10,710	95.4		23.8			99.6
CN 8098	11,070	10,600	68.3	11,090	10,570	95.4	10,760	10,730	68.2	10,780	10,710	95.4		145.7			99.7
CN 4944	11,070	10,680	68.2	11,080	10,590	95.4	10,760	10,730	68.2	10,780	10,710	95.4		153.1			99.7
CN 7618	11,070	10,680	68.3	11,090	10,590	95.4	10,760	10,730	68.2	10,780	10,710	95.4		149.6			99.7
CN 20608	11,070	10,700	68.1	11,090	10,610	95.3	10,760	10,730	68.2	10,780	10,710	95.4		135.7			99.7
Phase Jess																	
Boundary end of Lwando							10,770	10,730	68.2	10,790	10,710	95.4					99.6
Interval duration of Lwando									33		108	95.4					99.8
Span of dates of Lwando									16		53	95.4					99.9
CN 18638	10,710	10,590	68.2	10,780	10,510	95.4	10,780	10,740	68.2	10,860	10,720	95.4		27.4			99.5
CN 21323	10,750	10,590	68.2	11,070	10,560	95.4	10,780	10,740	68.2	10,860	10,720	95.4		69.8			99.4
CN 22339	11,060	10,590	68.2	11,070	10,570	95.4	10,780	10,740	68.2	10,860	10,720	95.4		106.7			99.4
Phase Lwando																	
Boundary start of Lwando							10,790	10,740	68.2	10,890	10,720	95.4					99.1
Interval Bonile									95		190	95.4					96.2
CN 501	11,090	10,790	68.3	11,120	10,760	95.4	10,940	10,750	68.2	10,980	10,740	95.4		100.1			96.8
Boundary end of Irit							11,040	10,750	68.2	11,040	10,740	95.4					97.1
Interval duration of Irit									83		201	95.4					98.5
Span of dates of Irit									38		131	95.4					99
CN 20408	11,060	10,690	68.2	11,070	10,610	95.4	11,040	10,950	68.2	11,050	10,740	95.4		65.9			98.2
CN 30047	11,070	10,710	68.2	11,100	10,660	95.4	11,040	10,950	68.2	11,050	10,740	95.4		111.9			97.9
CN 30048	11,070	10,760	68.2	11,100	10,710	95.4	11,040	10,950	68.2	11,050	10,740	95.4		113			97.7
Phase Irit																	
Boundary end of Irene							11,050	10,970	68.2	11,060	10,750	95.4					98.3
Interval duration of Irene									27		69	95.4					100
Span of dates of Irene									22		59	95.4					100

(Continued)

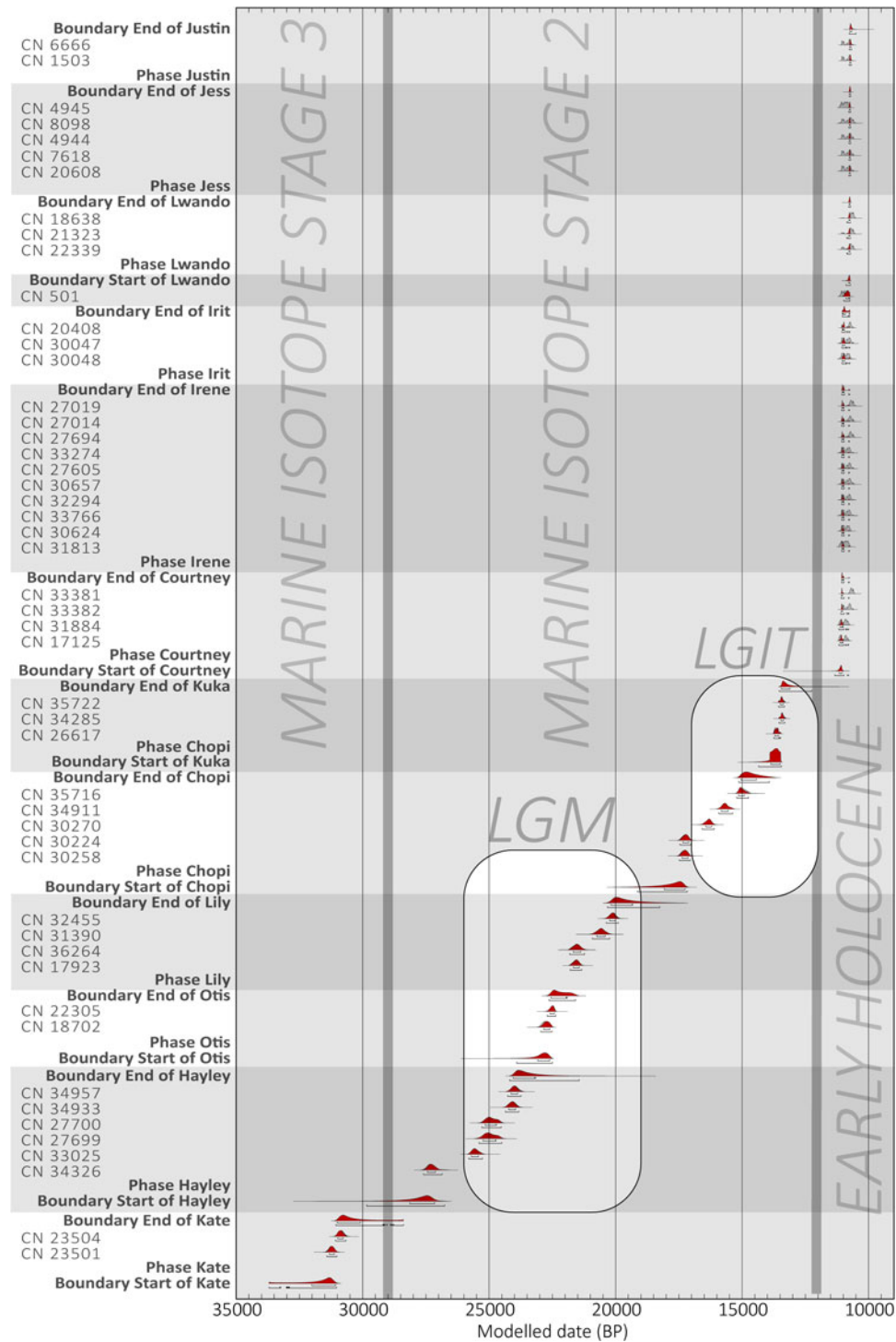
Table 2. Continued.

Name	Unmodeled (cal yr BP)						Modeled (cal yr BP)						Indices Amodel 54.1 Aoverall 54.1				
	From	To	%	From	To	%	From	To	%	From	To	%	Acomb	A	L	P	C
CN 27019	10,750	10,590	68.2	11,070	10,560	95.4	11,060	10,980	68.2	11,060	10,760	95.4		35.3			98.7
CN 27014	11,060	10,610	68.2	11,080	10,590	95.4	11,060	10,980	68.2	11,060	10,760	95.4		94.4			98.6
CN 27694	11,060	10,600	68.3	11,070	10,580	95.3	11,060	10,980	68.2	11,060	10,760	95.4		70.9			98.7
CN 33274	11,070	10,730	68.2	11,100	10,700	95.4	11,060	10,980	68.2	11,060	10,760	95.4		127.4			98.6
CN 27605	11,070	10,700	68.2	11,090	10,610	95.4	11,060	10,980	68.2	11,060	10,760	95.4		122			98.6
CN 30657	11,070	10,700	68.2	11,100	10,600	95.4	11,060	10,980	68.2	11,060	10,760	95.4		125.8			98.6
CN 32294	11,070	10,710	68.2	11,090	10,680	95.4	11,060	10,980	68.2	11,060	10,760	95.4		125.2			98.6
CN 33766	11,070	10,720	68.2	11,100	10,690	95.4	11,060	10,980	68.2	11,060	10,760	95.4		127.7			98.6
CN 30624	11,070	10,760	68.2	11,090	10,720	95.4	11,060	10,980	68.2	11,060	10,760	95.4		121.9			98.6
CN 31813	11,100	10,790	68.1	11,160	10,750	95.4	11,060	10,980	68.2	11,060	10,760	95.4		87			98.6
Phase Irene																	
Boundary end of Courtney							11,060	10,990	68.2	11,070	10,760	95.4					98.9
Interval duration of Courtney								116	68.2		349	95.4					99.6
Span of dates of Courtney								69	68.2		172	95.4					99.7
CN 33381	10,730	10,590	68.2	11,060	10,570	95.4	11,070	11,040	68.2	11,090	10,770	95.4		10			99.8
CN 33382	11,070	10,700	68.2	11,080	10,610	95.4	11,080	11,030	68.2	11,100	10,780	95.4		93.7			99.8
CN 31884	11,140	10,800	68.2	11,170	10,780	95.4	11,120	11,010	68.2	11,170	10,790	95.5		94.3			99.7
CN 17125	11,170	10,870	68.2	11,180	10,790	95.5	11,120	11,010	68.2	11,170	10,800	95.4		90.1			99.6
Phase Courtney																	
Boundary start of Courtney							11,160	11,050	68.2	11,340	10,800	95.4					99.6
Interval Kuka to Courtney							1984	2395	68.2	1077	2537	95.4					99.6
Boundary end of Kuka							13,470	13,130	68.2	13,550	12,270	95.4					99.4
Interval duration of Kuka							74	777	68.2		1792	95.4					99.6
Span of dates for Kuka							108	293	68.2	7	342	95.4					99.9
CN 26617	13,490	13,390	68.2	13,560	13,330	95.4	13,490	13,400	68.2	13,570	13,350	95.4		101.6			99.9
CN 35722	13,480	13,380	68.2	13,550	13,320	95.4	13,490	13,380	68.2	13,560	13,330	95.4		101.4			99.9
CN 34285	13,720	13,590	68.2	13,760	13,490	95.4	13,700	13,560	68.2	13,740	13,470	95.4		87.9			99.9
Phase Kuka																	
Boundary start of Kuka							13,880	13,510	68.2	14,360	13,470	95.4					99.8
Interval Chopi2Kuka							425	1277	68.2		1363	95.4					99.8
Boundary end of Chopi							15,050	14,380	68.2	15,130	13,840	95.4					99.8
Interval duration of Chopi							2470	3694	68.2	2234	4756	95.4					99.8
Span of dates for Chopi							2142	2445	68.2	2018	2622	95.4					99.9
CN 35716	15,130	14,870	68.2	15,200	14,710	95.4	15,140	14,910	68.2	15,210	14,750	95.4		103.4			99.9
CN 34911	15,820	15,550	68.2	15,920	15,370	95.4	15,820	15,550	68.2	15,920	15,370	95.4		99.9			99.9
CN 30270	16,430	16,200	68.2	16,580	16,100	95.4	16,430	16,200	68.2	16,580	16,100	95.4		100			99.9
CN 30224	17,360	17,120	68.2	17,470	17,030	95.4	17,340	17,110	68.2	17,460	17,020	95.4		101			99.9
CN 30258	17,400	17,160	68.2	17,500	17,060	95.4	17,380	17,150	68.2	17,490	17,050	95.4		100.8			99.9

(Continued)

Table 2. Continued.

Name	Unmodeled (cal yr BP)						Modeled (cal yr BP)						Indices Amodel 54.1 Aoverall 54.1				
	From	To	%	From	To	%	From	To	%	From	To	%	Acomb	A	L	P	C
Phase Chopi																	
Boundary start of Chopi							18,080	17,260	68.2	19,140	17,160	95.4					99.6
Interval Lily2Chopi							1146	2621	68.2	156	2773	95.4					99.6
Boundary end of Lily							20,190	19,340	68.2	20,320	18,260	95.4					99.6
Interval duration of Lily							1806	3023	68.2	1464	4044	95.4					99.8
Span of dates for Lily							1330	1645	68.2	1173	1799	95.4					99.9
CN 32455	20,220	19,990	68.2	20,350	19,880	95.4	20,240	20,010	68.2	20,370	19,900	95.4		98.3			99.9
CN 31390	20,750	20,420	68.2	20,920	20,240	95.4	20,750	20,420	68.2	20,920	20,240	95.4		100.1			99.8
CN 36264	21,690	21,390	68.2	21,830	21,240	95.4	21,680	21,380	68.2	21,820	21,240	95.4		100.8			99.8
CN 17923	21,680	21,440	68.2	21,800	21,350	95.4	21,670	21,440	68.2	21,800	21,340	95.4		100.6			99.9
Phase Lily																	
Boundary end of Otis							22,560	21,900	68.2	22,630	21,590	95.4					99.8
Interval duration of Otis							191	1178	68.2		1954	95.4					99.7
Span of dates for Otis								296	68.2		449	95.4					99.9
CN 22305	22,570	22,420	68.2	22,680	22,360	95.4	22,590	22,430	68.2	22,700	22,370	95.4		95.8			99.9
CN 18702	22,920	22,690	68.2	23,010	22,570	95.4	22,840	22,600	68.2	22,950	22,510	95.4		89.1			99.9
Phase Otis																	
Boundary start of Otis							23,080	22,600	68.2	23,920	22,500	95.4					99
Sequence LBCS-SRCS																	
Boundary end of Hayley							24,050	23,160	68.2	24,190	21,450	95.4					98.6
Interval duration of Hayley							3315	4985	68.2	2921	7544	95.4					98.7
Span of dates for Hayley							3110	3503	68.2	2839	3711	95.4					99.9
CN 34957	24,120	23,850	68.2	24,250	23,710	95.4	24,140	23,880	68.2	24,270	23,740	95.4		100.9			99.8
CN 34933	24,220	23,940	68.2	24,360	23,810	95.4	24,230	23,960	68.2	24,360	23,830	95.4		101.4			99.8
CN 27700	25,150	24,720	68.2	25,300	24,520	95.4	25,150	24,700	68.2	25,300	24,520	95.4		100			99.8
CN 27699	25,250	24,740	68.2	25,400	24,500	95.4	25,250	24,740	68.2	25,400	24,510	95.4		100			99.8
CN 33025	25,700	25,450	68.2	25,800	25,250	95.4	25,700	25,450	68.2	25,800	25,250	95.4		100			99.8
CN 34326	27,450	27,200	68.2	27,600	27,000	95.4	27,450	27,150	68.2	27,600	26,850	95.4		94.1			99.8
Phase Hayley																	
Boundary start of Hayley							28,100	27,150	68.2	29,800	26,750	95.4					98.5
Sequence LBCS-Hayley																	
Boundary end of Kate							31,000	30,100	68.2	31,050	28,400	95.4					99.3
Interval duration of Kate							188	1977	68.2		4290	95.4					99
Span of dates for Kate							196	498	68.2		623	95.4					99.9
CN 23504	30,950	30,750	68.2	31,050	30,650	95.4	31,000	30,800	68.2	31,050	30,650	95.4		97.1			99.9
CN 23501	31,350	31,150	68.2	31,450	31,050	95.4	31,300	31,100	68.2	31,400	31,000	95.4		96.2			99.9
Phase Kate																	
Boundary start of Kate							32,000	31,100	68.2	33,700	31,050	95.4					99.3
Sequence LBCS-Kate																	



**Figure 7.** Bayesian model results. This figure shows the results of a Markov Chain Monte Carlo analysis of the radiocarbon data from Waterfall Bluff at both 68.2% and 95.4% ranges. The samples are ordered in chrono-stratigraphic order. For all samples, the posterior density function and range are represented in red, and the unmodeled probability density function and range are represented in gray. The ranges of Marine Isotope Stage (MIS) 3, MIS 2, and the Early Holocene are demarcated with vertical gray bars, as are the last glacial maximum (LGM) and last glacial/interglacial transition (LGIT), showing which samples date to these time periods. Overall, the chronological sequence shows persistent occupation of the rock shelter from Late MIS 3 to the Early Holocene, including during the LGM and LGIT. (For interpretation of the references to color in this figure legend, the reader is referred to the web version of this article.)

using standard sample preparation procedures (Wintle, 1997; Aitken, 1998). Equivalent dose ( $D_e$ ) values were estimated for single grains using the single aliquot regenerative-dose

procedure (Galbraith et al., 1999; Murray and Wintle, 2000). Details about sample preparation, equipment, measurement, and data analysis procedures are provided in

Supplementary File 5. Grains with aberrant OSL properties were rejected from final  $D_e$  determination (Jacobs et al., 2008), following the rejection criteria outlined in Supplementary Table S5-2. Environmental dose rates were calculated as the sum of the external beta, gamma, and cosmic-ray dose rates and a small alpha dose-rate contribution from inside the mineral grains.

The accepted  $D_e$  values for individual grains from each sample are displayed on radial plots in Supplemental Figure S5-3. If the individual values are consistent with statistical expectations, then 95% of the points should scatter within a band  $\pm 2$  units wide, projecting from the “standardized estimate” axis on the left to any chosen  $D_e$  value on the radial axis to the right (Galbraith et al., 1999). It is apparent from the plots for each sample that the  $D_e$  estimates are spread widely and do not fall within a single band of  $\pm 2$  units. This spread is also indicated in the  $D_e$  overdispersion (OD) values (Table 3), which range from  $37 \pm 3\%$  (CN311) to  $50 \pm 6\%$  (CN312), and are much greater than the  $14 \pm 4\%$  OD value obtained for sample CN308 under controlled laboratory conditions in a dose recovery test (Supplemental Fig. S5-2). Two types of  $D_e$  distributions were observed for the Waterfall Bluff samples. The first type (sample CN311) shows a broad distribution that is scattered around a central value (Supplemental Fig. S5-3a). For this sample, we used the central age model (CAM) (Galbraith et al., 1999) to obtain a best-estimate final  $D_e$  value for age determination. The CAM takes into account the OD; the greater the OD, the larger the associated uncertainty on  $D_e$ . The second type (samples CN308, CN309, and CN312) also shows a broad distribution, but with a number of additional characteristics.

First, some grains have much higher than expected  $D_e$  values (up to  $\sim 225$  Gy). These high  $D_e$  values form part of a distribution of  $D_e$  values that is truncated at the upper end of the distribution (Supplemental Fig. S5-3c–e), excluding grains saturated with respect to dose (criteria 7 and 8 in Supplementary Table S5-2) from which no  $D_e$  value could be calculated. This means that the calculated OD values are minimum values only, and that the true spread in  $D_e$  values is greater than that observed in the radial plots.

Second, these samples also show no evidence for the presence of discrete  $D_e$  components. Instead, these samples have continuous  $D_e$  distributions that can be interpreted as evidence for either substantial bioturbation of sediments or partial bleaching of sediment, including the liberation of grains from roof spall. Sample CN310 has “transitional”  $D_e$  characteristics between these two types of distributions. For samples CN313, CN310, CN309, and CN308, further work on understanding site formation and sediment context at the microscopic level is required to make an informative interpretation of the  $D_e$  distributions and to help choose an appropriate age model for final  $D_e$  determination. In the absence of this information, we calculated both the CAM  $D_e$  value and a minimum  $D_e$  value, using the 3-parameter minimum age model (MAM) of Galbraith and colleagues (1999) for each of these samples (Table 3).

**Table 3.** Final environmental dose rate results,  $D_e$  values, and optically stimulated luminescence (OSL) ages for Waterfall Bluff samples.  $D_e$  and OSL age results using the 3-parameter minimum age model (MAM) (Galbraith et al., 1999) are given in addition to the central age model (CAM) (Galbraith et al., 1999) for samples CN308, CN309, CN310, and CN312. MAM OSL age determinations for these samples are currently assumed to be most representative of sample burial age but require further investigation.

Cat. number	Depth (m)	SubAgg	Field water content (%) <sup>a</sup>	Dose rates (Gy/ka)			Total dose rate (Gy/ka)	Number of grains	Age model	$D_e$ (Gy)	OD (%) <sup>b</sup>	OSL age (ka)
				Beta	Gamma	Cosmic						
309	0.57	LBCS Otis	10 (10.8)	0.397 $\pm$ 0.024	0.429 $\pm$ 0.021	0.052 $\pm$ 0.004	1.655 $\pm$ 0.049	317/3000	MAM	19.0 $\pm$ 1.8	36.7 $\pm$ 2.8	13.3 $\pm$ 0.7
				0.849 $\pm$ 0.031	0.578 $\pm$ 0.026	0.051 $\pm$ 0.004						
308	0.76	LBCS Kate	5 (5.4)	0.877 $\pm$ 0.037	0.695 $\pm$ 0.030	0.050 $\pm$ 0.004	1.809 $\pm$ 0.049	144/3000	CAM	66.1 $\pm$ 1.9	42.8 $\pm$ 2.3	39.9 $\pm$ 1.8
				0.989 $\pm$ 0.035	0.740 $\pm$ 0.033	0.048 $\pm$ 0.004						
312	0.82	LBCS Colton	5 (4.1)	1.058 $\pm$ 0.038	0.808 $\pm$ 0.035	0.047 $\pm$ 0.004	1.945 $\pm$ 0.052	66/2900	CAM	100.9 $\pm$ 7.4	49.5 $\pm$ 5.9	51.8 $\pm$ 4.2
				73.1 $\pm$ 7.9	37.6 $\pm$ 4.2							

<sup>a</sup>Estimated water content over period of burial of sample. Current measured field water content value given in brackets.

<sup>b</sup>Overdispersion (OD) values calculated using the CAM.

We calculated the beta and gamma dose rates for each of the samples using two different approaches. In one approach, we converted concentrations of U, Th, and K obtained from inductively coupled plasma mass spectrometry (ICP-MS) or optical emission spectroscopy (ICP-OES) to beta and gamma dose rates. In the other approach, we directly measured the beta dose rates using GM-25-5 beta counting (GMBC; Bøtter-Jensen and Mejdahl, 1988) and calculated the gamma dose rate from U and Th obtained through thick source alpha counting (TSAC) and K from a combination of GMBC and TSAC. Both approaches gave statistically consistent beta and gamma dose rates (average beta dose rate ratio =  $0.97 \pm 0.05$  and average gamma dose rate ratio =  $1.02 \pm 0.04$ ; Supplementary Tables S5-5, S5-6). For final age determination, we used the dose rate values derived from ICP-MS/ICP-OES (Table 3). There is a significant difference between the dose rates obtained for the samples from the shell- and clay-rich StratAgg SRCS (SubAgg Courtney) and the underlying LBCS sediments.

The final  $D_e$  values, environmental dose rates, and OSL ages for all five samples are listed in Table 3. To obtain an age for each sample, the model-derived  $D_e$  value was divided by the total environmental dose rate. For samples CN308, CN309, CN310, and CN312, the CAM  $D_e$  values result in significant overestimation of age when compared to AMS  $^{14}\text{C}$  ages. For these samples, the MAM  $D_e$  values instead gave ages that are in better agreement with those obtained by AMS  $^{14}\text{C}$  dating, suggesting that the sediment may have been partially bleached prior to deposition and burial. We caution that we need further information about the sedimentary context and site formation to be confident in the OSL ages for these sediments. Uncertainties on reported ages are given at the 1-sigma level.

## Chronology results

OSL dating (Table 3) and Bayesian  $^{14}\text{C}$  (see Table 2) modeled results are summarized below. The minimum age of sediment deposition for the currently deepest excavated deposits at Waterfall Bluff (LBCS Colton) have been OSL dated to  $37.6 \pm 4.2$  ka (CN312). Bayesian  $^{14}\text{C}$  model results for the start of overlying LBCS Kate range from 32,000 and 31,050 cal yr BP and end between 31,000 and 30,100 cal yr BP. These boundary age estimates are consistent with the minimum age of sediment deposition for LBCS Kate, OSL dated to  $27.8 \pm 2.1$  ka (CN308). Currently, no samples have been dated from LBCS Ollie, which directly overlays LBCS Kate. However, the next most recent deposit chronologically is LBCS Hayley, which has a lower Bayesian  $^{14}\text{C}$  model boundary result from 28,150 to 27,150 cal yr BP and an upper boundary from 24,050 to 23,160 cal yr BP.

Stratigraphically above LBCS Ollie is LBCS Otis. Bayesian  $^{14}\text{C}$  model results of the start of LBCS Otis range from 23,080 to 22,610 cal yr BP and end between 22,560 and 21,910 cal yr BP. These results are within the error range of the minimum age of sediment deposition for LBCS Otis, OSL dated to  $22.1 \pm 1.3$  ka (CN309).

Bayesian  $^{14}\text{C}$  model results for LBCS Lily, which overlays LBCS Otis, range from 22,560 to 21,910 cal yr BP and end between 20,190 and 19,330 cal yr BP. LBCS Chopi deposits are not laterally extensive but do overlay LBCS Lily. Bayesian  $^{14}\text{C}$  model results for LBCS Chopi range from 18,080 to 17,250 cal BP and end between 15,050 and 14,440 cal yr BP.

LBCS Kuka shares a lower boundary with LBCS Lily, LBCS Chopi, and LBCS Hayley deposits, underscoring the complex and spatially discrete distribution of the stratigraphy across the site. LBCS Kuka is also the uppermost SubAgg of the LBCS, and its upper boundary marks the transition to SRCS where it shares a boundary primarily with LBCS Courtney, but also SRCS Irene. Bayesian  $^{14}\text{C}$  model results for LBCS Kuka interpret the lower boundary to date from 14,070 to 13,570 cal yr BP and the upper boundary from 13,520 to 12,830 cal yr BP. This is consistent with the minimum age of sediment deposition given by CN310, OSL dated to  $12.5 \pm 1.2$  ka.

SubAgg Courtney is the stratigraphically deepest layer of the SRCS. Bayesian  $^{14}\text{C}$  model results date the lower SRCS Courtney boundary from 11,160 to 11,050 cal yr BP and the upper boundary between 11,060 and 10,990 cal yr BP. The OSL age of sample CN311 is slightly older than these results at  $13.3 \pm 0.7$  ka, a minor discrepancy that can be attributed to an increased potential for underestimation in beta dose rate calculations (and thus OSL age overestimation), caused by the shell-rich deposit (Cunningham, 2016).

Bayesian  $^{14}\text{C}$  model results for overlying SRCS layers have been calculated (in chronostratigraphic order) for SRCS Irene, Irit, Bonile, Lwando, Jess, and Justin. From SRCS Courtney to SRCS Justin, the Bayesian  $^{14}\text{C}$  model results calculate that these deposits formed in less than 450 years.

A later SRCS sequence dating to the Middle Holocene has been discovered in N844E335SW. AMS  $^{14}\text{C}$  dates from SRCS Josh and SRCS Nate have been dated to 8,395–8,203 cal yr BP and 8,288–8,025 cal yr BP, respectively. Since the relationship between these deposits and those in the main excavation area remain unknown, they were not used in the Bayesian model.

## ARCHAEOLOGICAL MATERIAL

To date, more than 25,000 individual artifacts, bone, ochre, and other archaeological remains have been plotted in 3D using total stations. These data provide detailed information on the spatio-temporal distribution of anthropogenic behaviors at the site. Here, we provide short summaries of the stone artifacts, anthropogenically modified bone and shell, marine shell, marine vertebrates, and fish remains with the intention of publishing more detailed descriptions about these assemblages, and the terrestrial fauna, once the analyses are completed.

## Lithics

In total, 403 lithics have been analyzed from the LBCS and SRCS to date. These data draw primarily on plotted cores

and flakes, omitting plotted flakes <5 mm in size and all sieved materials. The results provided here, therefore, should be considered preliminary given this limited sample and the absence of fine-mesh-sieved materials in the current analysis. We used a standardized attribute-based framework focused on variables to clarify strategies in raw material selection, reduction strategies, and techniques. The variables also help clarify two important aspects of lithic technology—the organization of technology and the size and shape of flakes. The LBCS sample comes predominantly from SubAggs Kuka, Lily, and Otis, while the SRCS sample draws largely from Bonile, Courtney, Jess, and Rosa. [Table 4](#) summarizes the lithic data by class and raw material within both the LBCS and SRCS. [Table 5](#) summarizes the proportions of cores versus flakes within the analyzed SubAggs. We have yet to analyze lithics from the deepest excavated deposits in LBCS Colton.

Hornfels is the dominant raw material used for lithic production in both LBCS (93.7%) and SRCS (85.7%) contexts, with chert, quartz, dolerite, and sandstone of minor importance. The relatively high frequency of retouched implements in both the LBCS (13.2%) and SRCS (12.4%) are made on hornfels. Cortex on the LBCS flakes is more angular (66.7%,  $n = 34$ ) than rounded (33.3%,  $n = 17$ ) compared to the SRCS where rounded cortex predominates (70.4%,  $n = 133$ ) over angular cortex (29.6%,  $n = 56$ ). Cortex retention is also greater on SRCS cores and flakes. Cores themselves comprise only a minor component of each assemblage; the LBCS member contains a single quartz bipolar core ([Fig. 8a](#)). Most of the SRCS cores (78%) are platform cores made on flat water-worn hornfels cobbles, flakes, and small (< 50 mm in maximum dimension) water-worn pebbles ([Fig. 9a–d](#)). The remaining 21% of SRCS cores was reduced using a bidirectional bipolar (hammer and anvil) strategy. Notably, one SRCS core was broken along the lateral edge and then flaked longitudinally along the broken edge to create elongated flakes and to refresh the edge for tasks that left the tool's edge marginally modified (see [Fig. 8d](#)). Additionally, the single LBCS core shows signs of platform-on-anvil technique (i.e., a freehand platform area opposed by a crushed distal core margin) specifically to produce elongated flakes (see [Fig. 8a](#)).

Flakes make up the majority of the lithic assemblages for both LBCS and SRCS. Comparisons of the SRCS and LBCS flake size (length and width) and elongation (length/width) show significantly larger and less elongated (i.e., wide and side-struck) flakes in the SRCS and smaller, more elongated flakes in the LBCS ( $F[1] = 15.22$ ,  $p < 0.01$ ; omega squared = 0.08). Several flakes in both the SRCS and LBCS assemblages show signs of bipolar damage (sheared bulbs of percussion and severe crushing) in their platform regions. The retouched tool frequencies are relatively high and similar between the LBCS and SRCS members. Scrapers and notched tools make up the majority of the formal tool inventory in both StratAggs. Scrapers are predominantly side and end forms, although this pattern is most common in the SRCS member with ~28% side, 21% end,

**Table 4.** Summary of Shell-Rich Clayey Sands (SRCS) and Light Brown Coarse Sands (LBCS) lithics. Counts and percentages of different lithic types and their raw materials within the two stratigraphic aggregates at Waterfall Bluff.

Stratigraphic aggregate	Lithic class	Raw material	n	%
<b>SRCS</b>	Minimally flaked units	Chert	1	0.7
		Dolerite	15	10.3
		Hornfels	125	86.2
	Flake fragments	Sandstone	4	2.8
		Dolerite	5	7.5
		Hornfels	55	82.1
		Quartzite	1	1.5
	Retouched	Sandstone	6	9.0
		Dolerite	2	5.9
	Cores	Hornfels	32	94.1
		Chert	1	6.7
		Hornfels	14	93.3
	Hammers/manuports	Hornfels	8	88.9
		Sandstone	1	11.1
	Groundstone	Hornfels	1	25.0
		Sandstone	3	75.0
	<b>Total SRCS</b>			<b>274</b>
<b>LBCS</b>	Minimally flaked units	Chert	1	1.7
		Dolerite	2	3.4
		Hornfels	56	94.9
	Flake fragments	Chert	1	1.9
		Dolerite	1	1.9
		Hornfels	48	92.3
		Quartz	1	1.9
	Retouched	Sandstone	1	1.9
		Hornfels	17	100.0
	Cores	Quartz	1	100.0
	<b>Total LBCS</b>			<b>129</b>

and 8% double (side and end) scrapers (see [Fig. 9e–g](#)). Scraper retouch is also steeper and more invasive in the SRCS member compared to the LBCS member, where edges show shallower scarring. Only one backed tool was found in the LBCS assemblage. Additionally, at least one of the LBCS flakes shows clear evidence of a step-terminating bending fracture at its distal end suggesting use in tasks with a high degree of bending tension (see [Fig. 8f](#)).

### Worked Bone

Bone is overall well preserved, but it varies in both LBCS and SRCS deposits based on proximity to the dripline where preservation is lower and sediments are largely de-calcified. Inside the dripline, bone and shell preservation rapidly improves and includes materials not limited to bone or teeth. For example, three preserved feathers have been recovered from SRCS Jess and SRCS Bonile.

A number of worked bone implements were shaped via cutting and abrasion ([Fig. 10](#)). Of particular interest is CN20667 (Lot 382) from SRCS Rosa (see [Fig. 10a](#)). The implement is 25 mm long, but it is broken. One side has

**Table 5.** Cores and Flakes in SRCS and LBCS. Distribution of cores and flakes with SubAggregates in the SRCS and LBCS.

Stratigraphic aggregate	Sub aggregate	Lithic class	n
<b>SRCS</b>	Bonile	Core	2
	Bonile	Flake	26
	Clara	Core	1
	Clara	Flake	4
	Courtney	Core	1
	Courtney	Flake	13
	Jess	Core	15
	Jess	Flake	147
	Josh	Flake	17
	Justin	Core	1
	Justin	Flake	4
	Lwando	Core	5
	Lwando	Flake	6
	Melanie	Flake	6
	Nate	Flake	1
	Rosa	Core	3
	Rosa	Flake	17
West	Flake	5	
	<b>SRCS total</b>		<b>274</b>
<b>LBCS</b>	Kate	Flake	3
	Kuka	Core	1
	Kuka	Flake	24
	Lily	Flake	14
	Ollie	Flake	14
	Otis	Flake	73
		<b>LBCS total</b>	

been abraded and cut to a conical point. Opposite the point at the thickest part of the tool are two parallel cuts that created an incision and stepped profile. The size and shape of the bone fragment is reminiscent of biconical fish gorges found in Holocene deposits elsewhere on South Africa's south coast (Bradfield, 2019). Association of this piece with fishing technology, however, remains tentative.

CN25758 (Lot 336) is from LBCS Kate (see Fig. 10b). It is a distal humerus of a rock hyrax (*Procavia capensis*) (S. Badenhorst, personal communication) that has been broken and faceted to create a bipointed keel on the shaft. Additionally, numerous beads have been found in SRCS Bonile and SRCS Josh that include 32 perforated tick shells (*Nassarius kraussianus*), perforated brown mussel shells (*Perna perna*), and one ostrich eggshell bead (*Struthio camelus*; CN26816, Lot 117; Fig. 11).

## Archaeomalacology

### Archaeomalacological methods

Whenever possible, marine shell remains have been identified to genus or species level (Kilburn and Rippey, 1982; Ridgway, 1998; Branch et al., 2010), from which minimum number of individuals (MNI) and weights were established. For bivalves, the highest number of either left or right hinges was used to determine the MNI. For limpets, and most whelks

and winkles, the number of apices was used to determine the MNI (Jerardino, 1997). In a few instances, MNI = 1 was established for a given species when no countable shell parts were encountered but taxonomically identifiable fragments were found. Each plotted shell fragment, whether countable or not, was weighed separately with a precision scale (0.01 g). Number of identified specimens or fragments (NISP) was also established.

Maximum shell lengths and widths were derived from brown mussels (*Perna perna*) where these were preserved. Shell limpet length and widths, plus others that can render full-length sizes via morphometric equations, were also obtained from limpet shells wherever possible (see, Jerardino and Navarro, 2008). Water-worn shells were also quantified and measured, and the species of origin was determined whenever possible. Preservation status of marine shell was further established via more qualitative evaluation of the degree of chalkiness or burning.

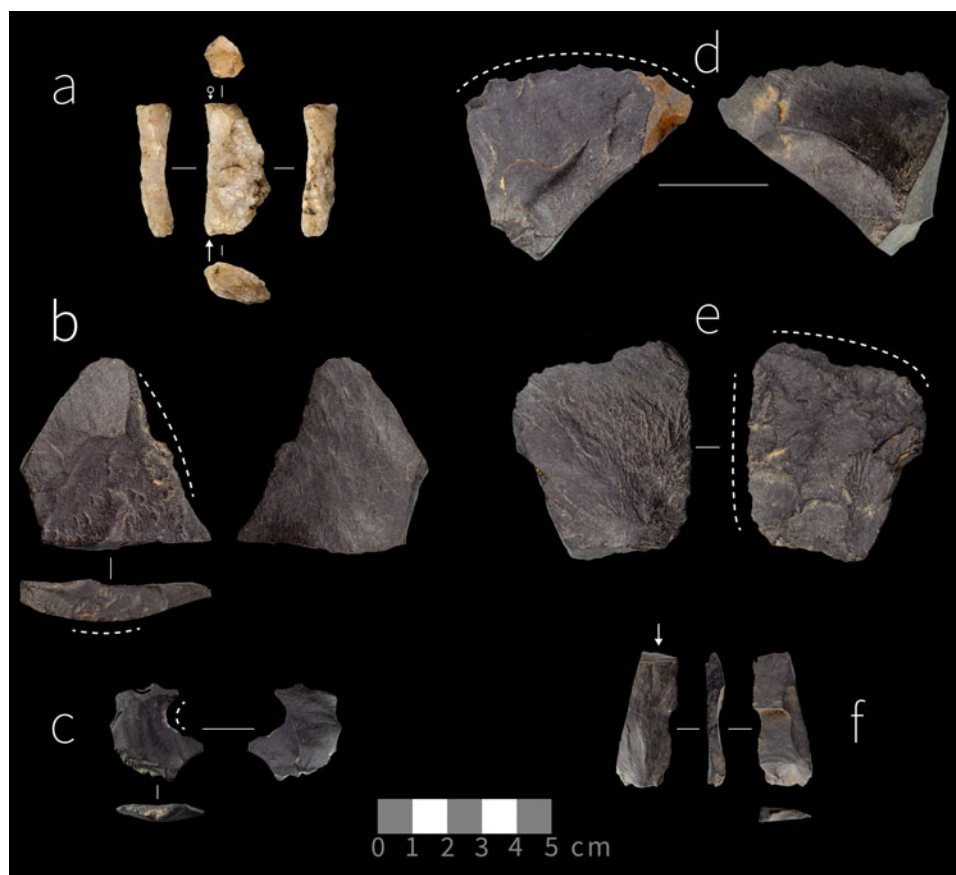
### Archaeomalacological preservation

LBCS shells (all analyzed SubAggs) show considerable fragmentation as evidenced by a high frequency of mussel fragments lacking hinges and having flat surfaces (Fig. 12). The majority of the shell currently recovered is from the 10-mm-sieve fraction. The deepest LBCS deposits are currently located at the dripline where there is visible evidence of decalcification. In one instance shellfish has been identified at a microscopic level using SEM and XRD. The sample, which was from LBCS Kuka, contained fragmented pieces of shell with clear nacre tablets, and XRD results showed high levels of calcite and aragonite, indicating recrystallized mussel shell (see Fig. 6).

Quantitatively, by dividing the total weight of each stratigraphic unit by the number of specimens (fragments and the few whole shells), SRCS Bonile is relatively less fragmented (3.7 g/specimen), followed by West (2.6), Courtney and Rosa (2.1, each), Jess upper (1.5), and Jess lower (1.4). Despite being the least fragmented among the studied SubAggs, shells from SRCS Bonile appear noticeably more burned than shells from any other SRCS SubAgg studied in this analysis, with the exception of SRCS Lwando (which was not studied). Quantitatively, 37.5% of the shell fragments from SRCS Bonile are burnt compared to <14.5% of shell fragments from the rest of the SRCS stratigraphic units. The label "burnt" refers to any visible exposure to heat, which is revealed in the change of color and/or luster of shells. For example, sometimes a shell outer surface may not become discolored but will lose its shine or gloss, while the inner surface can sometimes become beige or slightly grey in color. The green gloss that is so characteristic of brown mussels is also often lost or lessened as a result of heat exposure.

Another unique quality of the SRCS Bonile shells is that they appear to be preserving macrobotanical remains. During excavations, numerous whole and fragmentary leaves and grass stems were found adhering to the insides of mussel shells. In these cases, shells were often oriented with the cup





**Figure 8.** (color online) Sample of stone artifacts from LBCS. (a) anvil-supported bladelet core; (b) bipolar split flake with wear on the split surface; (c–e) notched flakes; (f) blade with bending fracture denoted by arrow. (a) made on quartz and (b–f) made on hornfels.

of the shell facing downward, and so we currently believe that the shells not only shielded the macrobotanical remains but may be creating unique microenvironments that inhibit deterioration of the plant tissues (e.g., Jerardino and Navarro, 2008).

SRCS Courtney specimens are powdery (chalky) and crumbly to different degrees yet appear unburnt. It is possible that the partial loss of the shell mineralogical structure in Courtney obscures the fact that they could have also been exposed to heat as in stratum Bonile. Additionally, marine shell remains from SRCS Jess were often chalky due to decomposition of the mineralogical shell structure and brittle compared to shell found in other SRCS SubAggs. The highly fragmented nature of the shell in SRCS Jess is also evidenced by a high frequency of mussel fragments lacking hinges and showing the greatest relative levels of fragmentation. Many fragments also had flat surfaces. This pattern is consistent with higher fragmentation rates due to longer exposure of shells on the site's surface and/or compression of the deposits (Jerardino, 2018).

#### Archaeomalacological observations

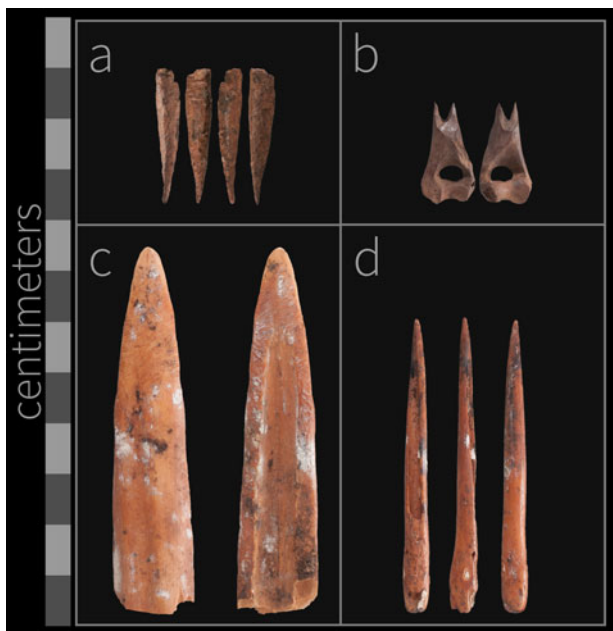
Sample sizes and percentages of marine shell species in terms of MNI and weights for SRCS samples are shown in Table 6. Sample sizes are rather small for meaningful calculations of percentages, with only two stratigraphic units in SRCS

represented by numbers above 100 individuals, namely SRCS West (MNI = 104) and Bonile (MNI = 267). The LBCS samples await full analysis, but some preliminary observations are available. The total shell fragment counts (NISP) are as follows: LBCS Chopi (21), LBCS Hayley (19), LBCS Kuka (shell remains only identified via SEM and XRD), LBCS Ollie (53), LBCS Kate (44), and LBCS Colton (8). No additional archaeomalacological observations are currently available for LBCS samples from the 2019 excavated deposits that greatly expanded the sample of LBCS materials.

Among the studied SRCS samples, 17 shellfish taxa were identified to genus and to broad taxonomic groups (see Table 6). Brown mussel (*Perna perna*) is the dominant species in the assemblage (70.0%–86.5% by MNI), with minor but noticeable contributions of small barnacles, oysters, and limpets. Taking into account the small number of measurable individuals (total  $n = 90$ , including left and right valves), most of the collected brown mussels that were brought back to Waterfall Bluff appear to be rather small or medium in size, measuring between 40 mm and 80 mm. Initial observations from LBCS samples appear to reflect the same species abundance profile, but full analyses will test these first observations and provide quantified data to compare with the younger SRCS samples. Other much-less-frequent species in the Waterfall Bluff record, like *Comus platyaulax*, *Nerita albicilla*, and *Mitra litterata*, may have been picked up by chance during



**Figure 9.** (color online) Sample of stone artifacts from the Shell-Rich Clayey Sands. (a) bipolar core on water-worn pebble; (b) platform core on thin water-worn pebble; (c) bipolar core on nodule; (d) core on flake with retouched edge; (e–g) naturally backed knives; (h) large flake on cobble; (i, j) small retouched water-worn cobbles. All lithics were made on hornfels.

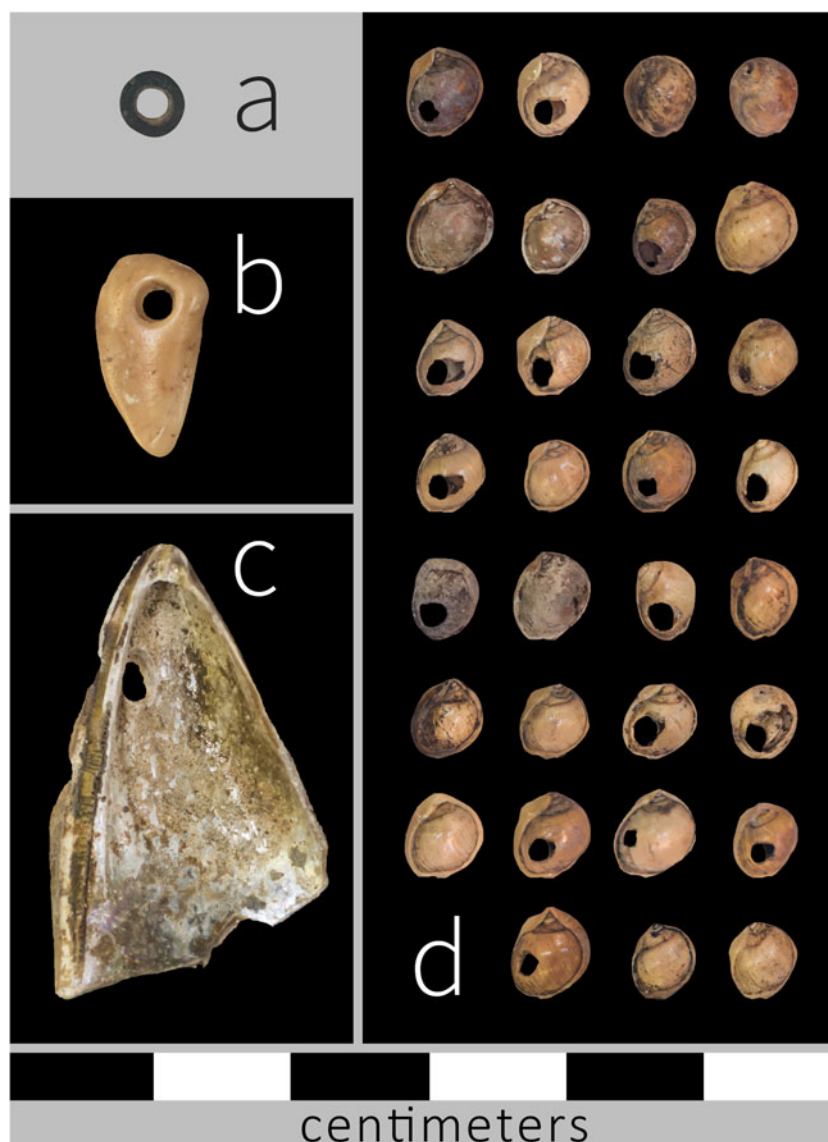


**Figure 10.** (color online) Sample of modified bone implements. (a) CN20667 (Lot 382; Shell-Rich Clayey Sands [SRCS] Rosa), possibly fish gorge; (b) CN25758 (Lot 336; Light Brown Coarse Sands [LBCS] Kate) broken and faceted distal humerus of a rock hyrax (*Procapra capensis*); (c) CN7500 (Lot 228; SRCS Jess) bifacial bone point; (d) CN7499 (Lot 228; SRCS Jess) abraded bone point.

foraging activities or as potential personal ornaments. Others are known to arrive to campsites clinging to other shells (i.e., *Helcion* sp., keyhole limpets, and barnacles) or attached to the byssus or threads of rocky shore mussels (i.e., *Barbatia obliquata*) (Jerardino, 2017). The latter species are all generally too small (<40 mm) for food consumption.

#### Water-worn shells

Water-worn shells (WWS) are organic macro-sediments that are often encountered with water-worn pebbles in many South African west-coast middens (Mbele et al., 2017). At Waterfall Bluff, these organic macro-sediments appear to derive mostly from the shells of oysters, and to a lesser extent from thick-shelled clams and scallops. Their sizes (3.1–45.2 mm) are larger than those observed for their equivalent on the west coast (2–20 mm) (Mbele et al., 2017). While the agency by which these sediments made their way to west-coast sites is largely understood, this is not yet the case for Waterfall Bluff organic macro-sediments, but hypothetical scenarios are discussed below. Water-worn pebbles were also encountered during the study of Waterfall Bluff shell samples, and they also constitute a part of the lithic assemblage. Several lithic artifacts were manufactured on small water-worn pebbles, suggesting that these secondary pebble sources likely



**Figure 11.** (color online) Perforated shells and beads from the Shell-Rich Clayey Sands (SRCS). (a) ostrich eggshell bead (*Struthio camelus*; CN26816, Lot 117, SRCS Josh); (b) perforated shell (*Perna perna*; CN26817; Lot 116, SRCS Bonile); (c) perforated shell (*Perna perna*; CN26818; Lot 116, SRCS Bonile); (d) perforated tick shells (*Nassarius kraussianus*; Lot 116, SRCS Bonile). The scale is the same for all objects in the figure.

served as a raw material source for toolmakers (see Fig. 9a, 9i, 9j). In order to quantify WWS abundance, a ratio was established ( $\text{ratio} = [\#WWS/MNI \text{ marine invertebrates}] \times 100$ ) and calculated for each stratigraphic unit. An overall average of 11.5 was established for SRCS samples. The strata with ratios around three times higher and more than the site's average were Jess (35.2) and Rosa (40.0), while those below the site's average correspond to the lowermost SRCS SubAggs, namely West (3.8), Bonile (4.1), and Courtney (7.3).

### Archaeoichthyofauna

Temperature, geology, and biological interactions are the three main influences on South African fish distributions, but

temperature is considered the most significant (Penrith, 1970; Turpie et al., 2000). There is an east–west gradient in fish species richness due largely to the impact of the warmer-water Agulhas current on the east coast, which provides a high-latitude habitat for tropical Indo-Pacific fish species within South Africa's subtropical east-coast waters (Turpie et al., 2000; Maggs, 2011). The east coast also has high species richness due to increased diversity in inshore habitats (Smith, 1980). Pondoland's sub-tidal habitat is composed of coast-parallel shelving reef complexes. There is a shift in benthic composition from algal-dominated reefs in the north to sponge- and ascidian-dominated communities in the south, with a major shift from Mbotyi southwards (Celliers et al., 2007). Celliers and colleagues (2007) attribute this shift to higher nutrient load from riverine runoff in the south.



**Figure 12.** (color online) Examples of Light Brown Coarse Sands (LBCS) shell remains. Assorted mussel and limpet shell remains from LBCS. (A) LBCS Ollie, Lot 320; (B) LBCS Kate, Lot 330; (C) LBCS Colton, Lot 342.

Today, eight species of fish account for 90% of the total estuarine fish catch (Maggs et al., 2013): *Chrysoblephus puniceus* (slinger seabream; Sparidae), *Galeichthys trowi* (Natal sea catfish; Ariidae), *Polysteganus praeorbitalis* (Scotsman seabream; Sparidae), *Lethrinus nebulosus* (green snapper; Lethrinidae), *Epinephelus marginatus* (dusky grouper; Serranidae), *Epinephelus andersoni* (cat-face rock-cod; Serranidae), *Epinephelus rivulatus* (halfmoon grouper; Serranidae), and *Cymatoceps nasutus* (black musselcracker; Sparidae). These fish belong to two main families: Sparidae and Serranidae.

### Archaeoichthyofaunal methods

The remains described here include plotted bones recovered from the 10 mm and 3 mm sieves. Fish remains from the 1.5-mm sieve have not yet been studied. Skeletal element terminology and calculations (NISP, %) were performed following standard zooarchaeological approaches and methods (Wheeler and Jones, 1976; Grayson, 1984; Cannon, 1987; Rojo, 1991; Reitz and Wing, 1999; Ramsey, 2009b). To visualize presentation of cranial and postcranial regions we grouped the skeletal elements according to these two groups and by eight anatomical regions (Butler, 1992; Amante and Eakins, 2009).

NISP was used as a basic quantitative unit for measuring counts, relative abundance, ordinal ranking, body part representation, spatial distribution, and taxonomic composition. To aid our taxonomic identifications, we have partnered with the East London Museum, the South African Institute for Aquatic Biodiversity, the Eastern Cape Parks and Tourism Agency, and the East London Aquarium to develop a reference collection of local fishes. Since the collection has only just started, we have not been able to identify most remains. We were able to do preliminary taxonomic identification for a few diagnostic bones (dentary, premaxilla) that were indicative at the family level.

Measurements were performed with a digital caliper on vertebrae centrum height, width, and length (Morales Muñoz and Rosenlund, 1979; Zohar et al., 1997; Zohar and Cooke, 2019), and on dentary and premaxilla length and height (Fig. 13). We also recorded the color of the bone, and signs of burning were identified on charred bones displaying black, gray, and white colors.

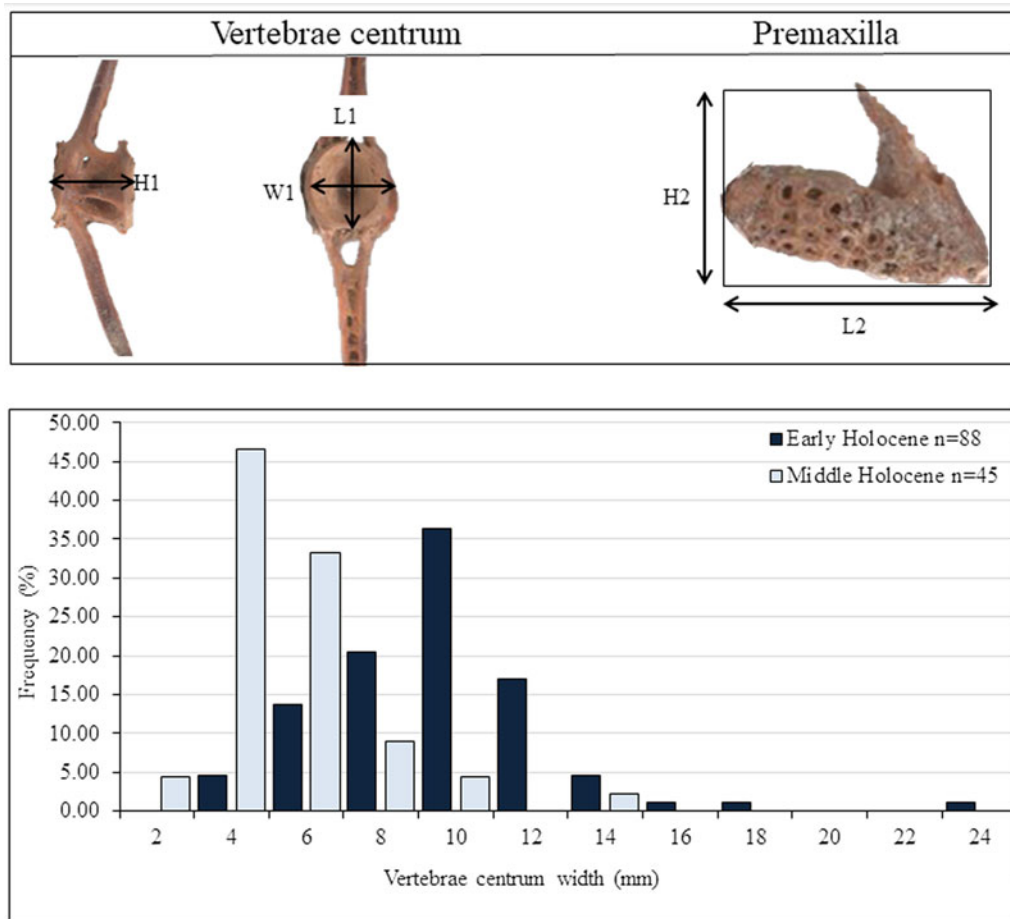
### Archaeoichthyofaunal results

Over 1,600 fish remains (NISP) have been identified to date from Waterfall Bluff, spanning LBCS SubAggs Kuka, Chopi, and Lily as well as all SubAggs in the SRCS. Most of the marine fish remains (69%; NISP = 1,108) are from SRCS SubAggs dated to the Early Holocene. The next greatest concentration of fish remains are found in the SRCS SubAggs dated to the Middle Holocene (31%; NISP = 492). Marine fish remains are also present in the LBCS (NISP = 4; 0.02%), but the sample is currently very small due to the limited LBCS excavations and sample that was available at the time of the analysis; the sample has been expanded since then.

Analysis of 767 skeletal elements sampled from SRCS show the presence of 73 different skeletal elements from the cranial and postcranial regions, including a single otolith from a very large fish (not yet identified) (Supplementary File 6). These data show that although the most abundant skeletal elements are vertebrae (37%, NISP = 287), in most SubAggs the cranial region is not underrepresented (Fig. 14). The poor preservation of bones from the branchial region is not surprising and supports our assumption that the fish were gutted in a different location, probably on the beach, close to their area of capture (Morales Muñoz and Rosenlund, 1979; Zohar and Cooke, 1997, 2019). Additionally, many of the fish remains are well preserved, including preservation of fragile features such as the vertebrae with haemal and neural spines (see Fig. 13 and Fig. 15).

**Table 6.** SRCS Shellfish. This table shows the species and common names of shellfish identified in Shell-Rich Clayey Sands (SRCS) deposits. The species are subdivided to show relative minimum number of individuals (MNI) and percentages by SubAggregate.

Species	Common name	Stratigraphic unit									
		SRCS									
		Jess		Rosa		West		Bonile		Courtney	
		MNI	%MNI	MNI	%MNI	MNI	%MNI	MNI	%MNI	MNI	%MNI
<b>MOLLUSCA</b>											
<i>Perna perna</i>	Brown mussel	55	77.5	7	70	90	86.5	222	83.5	33	80.5
Oyster (unid.)		2	2.8	-	0.0	1	1	1	0.4	1	2.4
<i>Comus platyaulax</i>	Comus venus shell	1	1.4	-	0.0	-	0.0	-	0.0	-	0.0
<i>Barbatia obliquata</i>	Oblique ark shell	2	2.8	-	0.0	-	0.0	-	0.0	-	0.0
<i>Scutellastra tabularis</i>	Giant limpet	0	0.0	1	10	3	2.9	-	0.0	-	0.0
<i>Scutellastra argenvillei</i>	Argenville's limpet	1	1.4	-	0.0	1	1	2	0.8	-	0.0
<i>Scutellastra barbara</i>	Bearded limpet	0	0.0	-	0.0	-	0.0	1	0.4	-	0.0
<i>Cymbula miniata</i>	Pink-rayed limpet	0	0.0	2	20	-	0.0	-	0.0	-	0.0
<i>Helcion sp.</i>	Rayed limpet	0	0.0	-	0.0	1	1	-	0.0	-	0.0
Limpet (unid.)		1	1.4	-	0.0	-	0.0	1	0.4	1	2.4
Keyhole limpet (unid.)		0	0.0	-	0.0	-	0.0	1	0.4	-	0.0
<i>Burnupena lagenaria</i>	Whelk	0	0.0	-	0.0	-	0.0	1	0.4	-	0.0
<i>Nerita albicilla</i>	Blotched nerite	0	0.0	-	0.0	-	0.0	2	0.8	-	0.0
<i>Mitra litterata</i>	Mitra	2	2.8	-	0.0	-	0.0	-	0.0	-	0.0
Whelk (unid.)		1	1.4	-	0.0	1	1	-	0.0	-	0.0
Unidentified mollusk		1	1.4	-	0.0	-	0.0	2	0.8	1	2.4
<b>ECHINODERMATA</b>											
Barnacles	Shore barnacles	0	0.0	-	0.0	-	0.0	-	0.0	-	0.0
		5	7.0	-	0.0	7	6.7	33	12.4	5	12.2
<b>Total</b>		<b>71</b>	<b>100</b>	<b>10</b>	<b>100</b>	<b>104</b>	<b>100</b>	<b>266</b>	<b>100</b>	<b>41</b>	<b>100</b>



**Figure 13.** (color online) Early and Middle Holocene fish vertebrae dimensions. This figure shows the distribution of fish vertebrae centrum width for Early Holocene and Middle Holocene assemblages with reference photos showing how the measurements were collected. The data suggest larger fish were collected during the Early Holocene.

Species-specific measurements of fish vertebra are well known to correlate to the overall size of the fish (Granadeiro and Silva, 2000). We measured the vertebrae centrum diameter (maximum length, width, and height) on a small sample (NISP = 133) from SRCS SubAggs attributed to either the Early Holocene (NISP = 88) or Middle Holocene (NISP = 45) (see Fig. 13). This analysis combines different species, so it only provides preliminary information on the relative sizes of the fishes that are represented in the assemblage. The observed SRCS pattern shows that all size groups of fishes are present, ranging from small (less than 10 cm in total length) to large fish (> 70 cm in total length). Larger fish are more abundant in the Early Holocene sample compared to the Middle Holocene sample (see Fig. 13). Future analysis will enable us to examine whether the reduction in fish size observed between Early and Middle Holocene samples accords with changes in fish population or changes in human exploitation patterns, or if it is biased due to sample sizes.

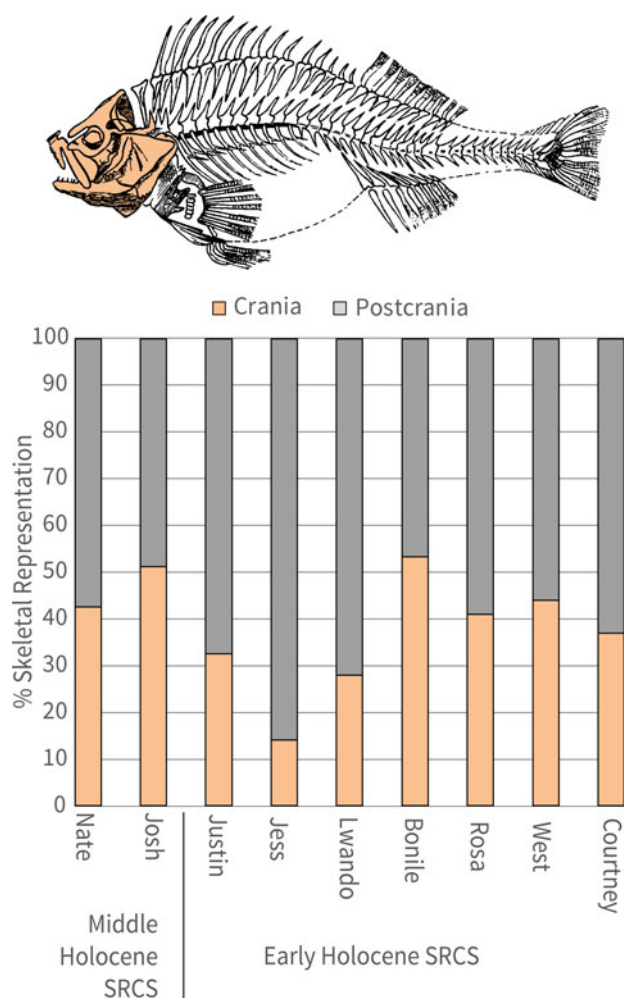
Taxonomic identification is currently in progress. So far, identifications at the family level include the following (in descending order): Sparidae (sea breams and porgies), Mugilidae (mulletts), Sciaenidae (drums), Haemulidae (grunters), Serranidae (groupers), Carangidae (jacks), and Labridae

(wrasses). Species of these families are among the most common fish captured in this area today (Maggs, 2011), and they are particularly common in littoral zones within estuaries and can tolerate both brackish and salt water. Additionally, we have identified the remains of crab (spp. unidentified) and spiny lobster (spp. unidentified).

## DISCUSSION

At Waterfall Bluff, groups of hunter-gatherers occupied the site during both glacial and interglacial periods. The narrow and steep continental shelf kept coastlines within a maximum distance of 10 km from the site (and likely only ~8 km) even during the LGM, but these distances still appear to have impacted people's use of the site and the region's resources. Nevertheless, these occupations provide an unprecedented opportunity to study hunter-gatherer behavioral variability in a relatively persistent coastal context across a glacial/interglacial cycle.

The detailed OSL and AMS  $^{14}\text{C}$  dating results at Waterfall Bluff provide independent and reliable chronological assessments of the stratigraphic sequence. The Waterfall Bluff chronology is now one of the most robust sequences dating to the



**Figure 14.** (color online) Percentage of preserved fish crania vs. postcrania. This chart shows the relative percentage of crania vs. post-crania in the Waterfall Bluff Shell-Rich Clayey Sands (SRCS) fish assemblage from 9 SubAggregates dating to the Middle Holocene and Early Holocene.

Pleistocene/Holocene transition in southern Africa, and our results demonstrate that there was neither a significant sedimentological nor occupational hiatus at the site from late MIS 3 to the Holocene, including during the LGM and LGIT. Current OSL dating results suggest the oldest current LBCS unit, Colton, starts ca. 38 ka and, along with LBCS Kate, these SubAggs currently comprise the MIS 3 sample. Thereafter, LBCS Hayley, Otis, and Lily formed during the LGM, while LBCS Chopi and Kuka date to the LGIT within MIS 2. LBCS Ollie, stratigraphically located between LBCS Kate and LBCS Otis, is currently undated, and therefore it is unknown whether it is associated with the underlying MIS 3 layers or the overlying LGM layers.

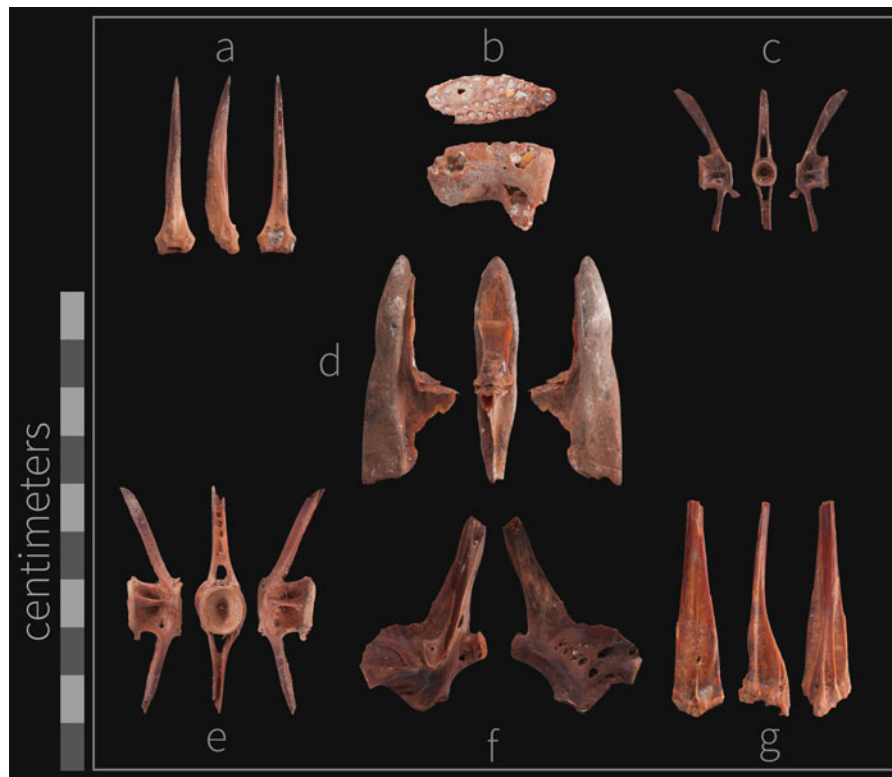
All LBCS deposits are characterized by coarse-grained, roofspall-rich sands. There are also isolated bands of darker, decalcified sediments (e.g., LBCS Ollie and Lily) within LBCS that contain stratified combustion features, and the LBCS stratigraphy is significantly better preserved farther inside the rock shelter where excavations are ongoing. Overlying LBCS, the SRCS shows a sedimentological change to

clay-rich deposits. The earliest known SRCS occupations (SRCS Courtney and Irene) are found stratified above the LBCS deposits in the main excavation area. This contact between the coarse-grain LBCS sands and the clay-rich SRCS is very distinct, and ongoing micromorphological studies are providing more information about this contact. The modeled radiocarbon dates for the SRCS suggest a tightly constrained occupation of the site from ca. 11,000 cal yr BP to ca. 10,500 cal yr BP during the Early Holocene. There is also evidence for Middle Holocene occupations at the site in N844E335SW, but their relationship to other SRCS stratigraphy remains unknown.

The radiocarbon dating within SRCS presents some unique challenges because the calibration curve intersects 3 times over a 500-year period for all SRCS results. As a result, the span of SRCS ages appears largely homogenized, which may be due to potentially small deviations that tip the whole set of SubAggs to the older or younger side of the wiggle. Nonetheless, our modeling results show a subtle shift from older dates to younger dates in stratigraphic continuity with the sequence, and we trust the age of the SRCS overall even if differences between SRCS SubAggs are currently difficult to identify.

The character of the SRCS, and the narrow time span of the ages, strongly suggests that these deposits represent one or more tightly packed occupations at the site, though the duration and timing of the occupations is unknown. There is abundant evidence that during these occupations earlier and contemporaneous deposits were dug out and/or modified. For example, SRCS Bonile was dug out toward the mouth of the rock shelter to make room for the deposition of SRCS Lwando. The shells within SRCS Lwando all have a characteristic grey coloration indicative of being heavily burnt, yet there is little *in situ* evidence of stratified combustion features or the remains of these features (e.g., ash and charcoal). Therefore, it appears that after SRCS Bonile was dug out, the SRCS Lwando shell itself was secondarily deposited from another location. In another example, numerous vertical infillings ~8 cm in diameter and ~20 cm deep have been excavated in SRCS West; these infillings extend downward and cut into SRCS Irene. These vertical structures are localized at the site and appear to have some spatial patterning to them, suggesting it may be the remains of emplaced posts for as-yet-unknown purposes. Analysis of the sediments within these vertical structures is also ongoing.

Stone artifacts are found throughout the LBCS and SRCS deposits at Waterfall Bluff. However, preliminary observations suggest that the lithics and other anthropogenic and faunal materials are less abundant in the deepest LBCS layers dating to MIS 3 compared to the LGM or LGIT layers. This could be due to changes in human occupation, taphonomic effects, or the limited sample of the lowest LBCS. The sample of LBCS described here, for example, comes from just the earliest excavations into LBCS from 2016 that together only amounted to 0.18 m<sup>3</sup>, which is roughly equivalent to an excavation 1 m × 0.5 m × 0.35 m. In comparison,



**Figure 15.** (color online) Examples of preserved fish bones from Waterfall Bluff. (a) Fish spine (CN471, Lot 107 Shell-Rich Clayey Sands [SRCS] Nate); (b) Sparidae premaxilla (CN10932, Lot 106, SRCS Nate); (c) vertebra CCN12124; Lot 115, SRCS Josh); (d) occipital crest (CN26765, Lot 266, SRCS West); (e) vertebra (CN2167, Lot 107, SRCS Nate); (f) hyomandibular (CN493, Lot 114, SRCS Bonile); (g) 1<sup>st</sup> dorsal pterygiophore (CN466, Lot 123, SRCS Josh).

0.77 m<sup>3</sup> was excavated from SRCS during that same time-frame, representing over four times more material recovered from SRCS than all of the LBCS. Subsequent excavations in 2019 have significantly increased the LBCS sample (largely unanalyzed) and with it our understanding of the human occupations from these layers.

Both LGM and Early Holocene assemblages are dominated by the use of hornfels, which is found throughout the region in terrestrial-contact metamorphic contexts, but it is also commonly washed down rivers and onto beaches. Differences in cortex types (rounded vs. angular) suggests toolmakers may have targeted more rounded riverine or weathered coastal raw material sources during the Early Holocene versus more terrestrial sources during the LGM when the coastline was ~8 km from the site. If this observation is verified in future analyses, then it will show that raw material procurement patterns were tethered to Pondoland's shifting coastline.

The presence of higher cortex retention rates in the Early Holocene compared to the LGM deposits suggests differences in LGM and Early Holocene flaking technologies. Early Holocene toolmakers may have initiated flaking more often on-site or reduced cores less intensively, or they may not have fully exploited cortical surfaces compared to LGM toolmakers. Lithic reduction and modification patterns further suggest that Waterfall Bluff toolmakers cycled lithics through several stages and applied techniques that included

using the same lithic pieces as both cores and implements. One Early Holocene core, for example, was broken along the lateral edge and then flaked longitudinally along the broken edge to create elongated flakes and to refresh the edge for tasks that left the tool's edge marginally modified. Additionally, a core from the LGM shows signs of platform-on-anvil technique (i.e., a freehand platform area opposed by a crushed distal core margin) specifically to maximize flaking potential and the production of elongated flakes (see Fig. 8a). Preliminary observations of the macro damage to the flakes show that at least one of the LBCS flakes has clear evidence of a step-terminating bending fracture at its distal end suggesting use in tasks with a high degree of bending tension. These tasks may have included the use of stone implements to pry open shellfish or to dislodge them from rocks. Future work will focus on testing this hypothesis.

### Coastal foraging from the late Pleistocene to the Holocene

Across southern Africa, evidence of coastal foraging during MIS 3 and MIS 2 (including the LGM) is largely absent. There are preliminary reports of shellfish in deposits dating from ca. 35 ka to ca. 26 ka at the site of Knysna Eastern Heads 1 (KEH1), on South Africa's south coast, but these data are currently unpublished (N. Cleghorn personal



communication, but see also Keller et al., 2019). Initially, the coastline would have only been ~10 km away from KEH1, but as sea levels continued to drop through MIS 3 the coastline all along the south coast expanded outward by over 20 km leaving KEH1 and other contemporaneous coastal sites, like Klipdrift, Nelson Bay Cave, and Matjies River, as inland locations (see Fig. 1). A similar situation occurred on the west coast where once-nearby coastlines were relocated well over 20 km away from sites such as Elands Bay Cave during MIS 3. By the LGM, all documented sites on the south and west coasts of southern Africa were between 50 km and more than 100 km away from the coastline (Fisher et al., 2010). Traces of marine mollusks and fish used as food sources are not seen in archaeological records during this period; they only appear in very small quantities at Byneskranskop in deposits dated ~17 ka (Schweitzer and Wilson, 1982). Exploitation of marine mollusks, marine mammals, and marine fish is not reported at other west- and south-coast sites until ~14 ka, when quantities progressively increased into the Holocene in step with rising sea levels and transgressing coastlines (Fig. 16). The lack of marine resources used as food sources in later MIS 3 and LGM deposits from currently coastal sites therefore suggests that the coast was simply too far from the sites on the south and west coasts to exploit. This does not seem to be the case at Waterfall Bluff where the coastline was ~8 km from the site during MIS 3 and the LGM due to the narrow continental shelf.

Shellfish and/or fish remains are found in nearly all the anthropogenic deposits at Waterfall Bluff to varying degrees, though the more extensive 2019 LBCS excavated remains are unanalyzed and unreported here. The presence of the shellfish and fish in deposits dated to the LGM alone is important because it is the first time that direct evidence of coastal foraging activities has been observed in southern Africa from deposits dating to a glacial maximum. However, there is very little else that can be said about how hunter-gatherers were utilizing aquatic resources during the LGM at this time. The reason is threefold. First, as was noted above, the LBCS assemblages presented here derive only from the earliest excavations into LBCS from 2016, and so they were very limited (<1 m<sup>3</sup>) and four times smaller than the contemporary SRCS excavations. This is due simply to the deeper and harder-to-reach nature of the LBCS deposits, and it is already being rectified by new excavations. Second, that sample of 2016 LBCS material was also collected almost exclusively from the dripline where there were clear taphonomic influences on the deposits from drip water, discoloring all sediments through the post-depositional process of decalcification. SRCS Jess, for example, is an easily identifiable marker-horizon across the excavations, being composed of golden-colored *Perna perna* shells in a dense shell-supported matrix. Yet at the dripline the layer has a dark black/brown coloration lacking shell (see Fig. 4). LBCS Lily and Ollie have similar dark colorations at the dripline and SEM/XRD analyses of a sediment sample from LBCS Kuka has found microscopic traces of partly dissolved shell (see Fig. 4 and Fig. 6). The implication is that both LBCS and SRCS deposits

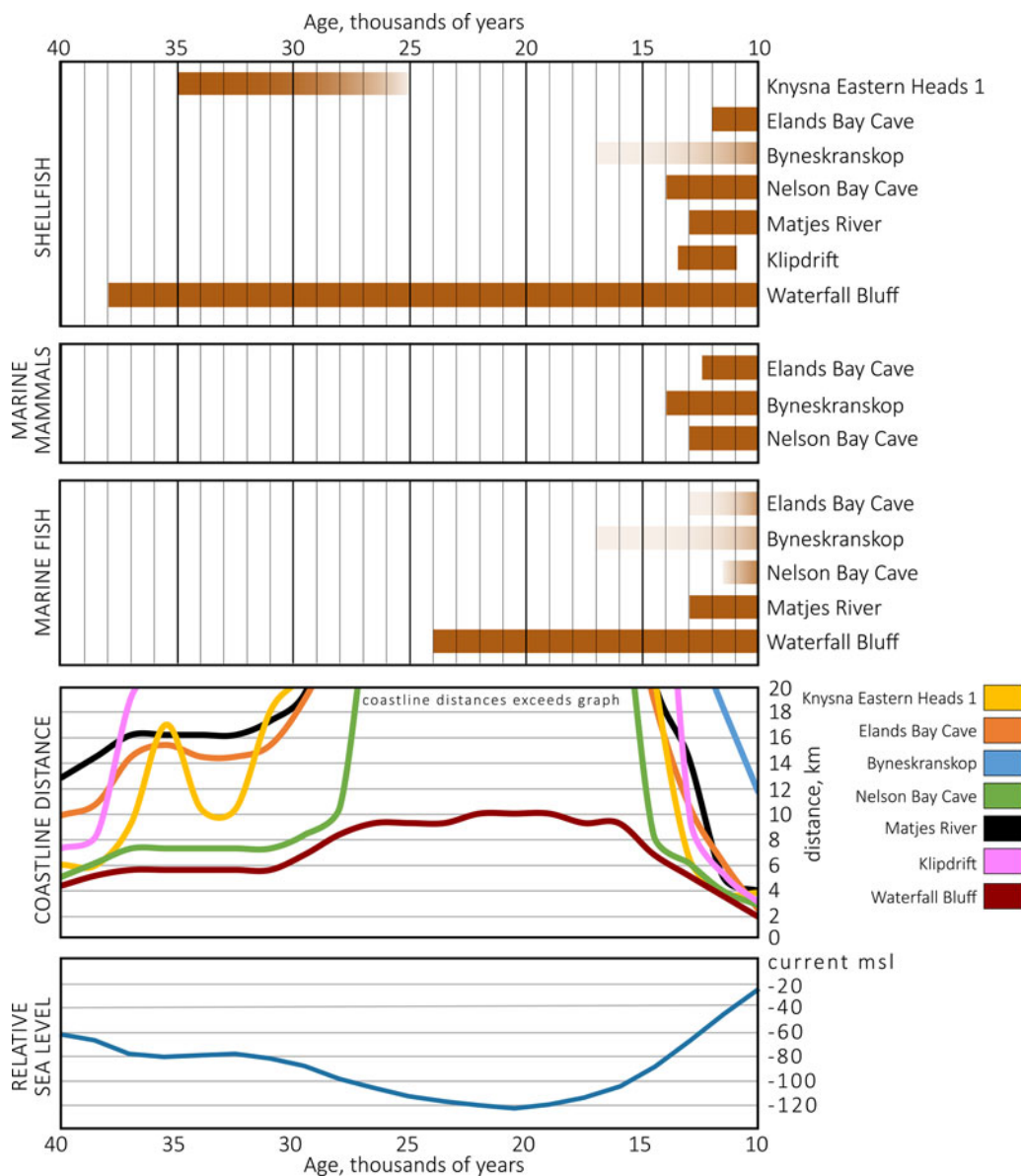
at the dripline may have once contained much greater quantities of shell that were likely removed through the process of dissolution via drip water.

A third possibility is that coastal foraging strategies and the human occupation of the rock shelter differed between the LGM and Holocene. The LBCS lithic assemblage, dating to the LGM, shows an increase in cortex signatures in cores and flakes, suggesting raw material sourcing away from shorelines or river mouths. Additionally, the presence of bipolar reduction, emphasizing the production of small flakes and bladelets, points to increased reduction intensity of stone nodules. Elsewhere these kinds of patterns have been linked to greater group mobility (Jerardino and Navarro, 2008).

The multi-proxy paleoenvironmental data described in Esteban et al. (2019) suggests a mosaic of open woodland vegetation and afrotemperate forests probably located in fire- and wind-protected cliffs and valleys on the exposed coastal plain during MIS 3 and the LGM when the coastline was between ~3 km and ~8 km from the site, respectively. During this time the climate was likely characterized by low rainfall seasonality and intensity but had sufficient perennial moisture availability to allow forest development. This started to change during the LGIT and the Early Holocene when multi-proxy evidence suggests higher rainfall intensity and seasonality (i.e., higher summer rainfall) coeval with evidence for forest retreat and open-land indicators like the expansion of mesic environments similar to those present in the region today.

These patterns establish a baseline for inferring changes in site occupation and coastal resource exploitation. Preliminary analysis of the fish remains shows abundance of Sparidae and Mugilidae, two families of fish that are known to occupy estuarine or brackish environments. These families are still abundant today and exploited by traditional fishing communities that harvest these fish from the mouths of nearby rivers like the Lupathana, Mkwani, and Msikaba (Turpie et al., 2000; Maggs, 2011). These environments also often provide rocky outcrops that support dense shellfish populations. In the SRCS Early Holocene deposits, the fish assemblage shows evidence of both cranial and post-cranial remains suggesting nearby procurement and on-site processing. Similarly, the abundance of whole shells throughout the SRCS implies on-site processing of shellfish in post-glacial deposits that is consistent with a nearshore context. Likewise, the exploitation of coastal forests and forest margins for wood-fuel, and perhaps other purposes, is also observed in the charcoal record (Esteban et al., 2019).

Marine geoscience data of the seafloor near Waterfall Bluff shows the presence of submarine canyons linked to many modern river systems (e.g., Umzimvubu, Msikaba, Mtentu, and Tezana Rivers) in the area (see Fig. 1). These canyons were formed by paleorivers that would have been active during glacial periods when the narrow continental shelf was exposed by lower sea levels. The canyons are believed to have supported forest ecosystems during MIS 3 and the LGM, as described in the *Podocarpus/Afrocarpus* pollen record by Esteban et al. (2019), while the rivers would have



**Figure 16.** (color online) Archaeological evidence of coastal foraging 40 ka to 10 ka. This figure shows the distribution of marine shellfish, marine mammals, and marine fish that have been documented at archaeological sites along the coast of South Africa. Excepting Waterfall Bluff, evidence of marine resource procurement disappears by 25 ka and reappears only ~15 ka, corresponding very closely to glacial/interglacial sea level fluctuations that impacted the locations of coastlines. Coastline distance is derived from Fisher and colleagues (2010), showing linear minimum distances to coastlines from sites through time. Relative sea level is adapted from Waelbroeck and colleagues (2002).

provided a ready supply of freshwater to support hunter-gatherers. These river systems also would have supported brackish estuarine habitats at river mouths for fishing adjacent to rocky coastlines supporting shellfish. We hypothesize that during the LGM, when the coastline was ~8 km away from the site, coastal foragers probably targeted these estuarine environments where field processing of fish would have been more common (e.g., salted, dried) and the meat either consumed immediately or transported back to the site (Zohar and Cooke, 2019). Shell fishing may not have been so tethered to rocky shores adjacent to river mouths but would have been possible all along the nearby coastline. As is the case today, it is very possible that the nearby rocky

shoreline was dominated by mussel beds during the entire site occupation. The archaeomalacological record from Waterfall Bluff shows that shellfish collection efforts were almost entirely geared toward the collection of brown mussels (>70% by MNI), with very sporadic pickings of oysters, limpets and whelks.

By and large, people's foraging rounds seem to have been limited to the mid-intertidal zone as evidenced by the medium-sized mussels. Ecological studies show that smaller brown mussels are more abundant upshore, while the opposite is the case for larger mussels (van Erkom Schurink and Griffiths, 1993; McQuaid et al., 2000). Hence, compared with the maximum sizes of up to 110 mm and 130 mm

currently reached by brown mussels near Port Alfred and East London (McQuaid et al., 2000), most of the collected mussels brought back to Waterfall Bluff appear to be rather small or medium in size.

Alternatively, we hypothesize that most large brown mussels were field processed before transport to the rock shelter. Ongoing archaeomalacological studies will likely shed further light on this topic. The implication is that catches of mollusks were either taken back whole to the site or shucked in various proportions before their transport to Waterfall Bluff. Some of them might also have also been consumed at processing points. This hypothesis is supported by both ethnographic observations and archaeological evidence for distance-based field processing of coastal resources (Bird and Bliege Bird, 1997; Zohar and Cooke, 1997; Bird et al., 2002; Jerardino, 2016b). We predict that the archaeological signature of this pattern, therefore, would show lower amounts of shell and higher shell fragmentation, and the fish would show the absence of discarded areas like the branchial region during the LGM and perhaps also the LGIT. The implications of this are more field processing and transportation of coastal resources to Waterfall Bluff depending on how distant the site was from coastlines through time. The preservation of fragile structures on the fish bones—like vertebrae with haemal and neural spines—further suggests that they were either protected via rapid deposition, preventing predator scavenging, and/or that the site was abandoned soon after the fish were processed. Therefore, visits to the site may have been brief, and perhaps for specific purposes such as fish/shell processing and consumption, before the hunter-gatherer groups moved on to other encampments. These patterns support historical documentation that show foraging communities from the wider region using the Pondoland and Kwa-Zulu Natal coastlines for short-lived logistical forays to collect specific plant and animal resources lacking in other parts of the region (Wright, 1971).

### Linking the coast to the hinterland

The timing of occupation at Waterfall Bluff hints at region-wide behavioral patterning that may link coastal and inland foraging groups. In the nearby Maloti-Drakensberg region and other inland areas, prehistoric activity is documented at Rose Cottage Cave, Ha Makotoko, Strathalan B, and Sehonghong before the onset of the LGM (Opperman, 1996; Pargeter et al., 2017; Stewart and Mitchell, 2018; Loftus et al., 2019). At Grassridge Rock Shelter in the Eastern Cape an occupation hiatus is recorded after 39.9–36.8 ka (Opperman, 1984; Collins et al., 2017), and hiatuses are also recorded at Sehonghong (Lesotho) and Rose Cottage Cave (Free State) between ca. 29 and 25 ka (Pargeter et al., 2017; Loftus et al., 2019). Likewise, there is also an occupational hiatus at Umbeli Belli in KwaZulu-Natal between ca. 24.9 and ca. 17.8 ka (Bader et al., 2016). Only at Umhlatuzana (Kaplan, 1990) and Shongweni (Vogel et al., 1986), both ~30 km inland of Durban, is occupation evident just prior to the LGM. At best, Umhlatuzana and Shongweni suggest that

people were sporadically present some 30 km inland of the present coastline just before and—more convincingly—after the LGM. Similarly, the patterning in the distribution of radiocarbon dates from Sehonghong suggests that during the early LGM, ca. 24–23 ka, the Lesotho highlands offered increased opportunities for hunter-gatherers, but only before conditions deteriorated sufficiently to discourage further occupation (Pargeter et al., 2017). While the regional record shows a lack of occupation during the LGM, the archaeological records from Waterfall Bluff shows evidence for human occupation in near-coastal contexts (see Fig. 7 and Fig. 16). Without excluding the possibility of human movement into lowland Lesotho and the eastern Free State during these times (cf. Stewart and Mitchell, 2016), our data show that some populations likely also migrated eastward to the coastline.

An uptick in human activity occurred across the region ca. 11 ka, with peaks in archaeological occupation at Ha Makotoko and Ntloana Tšoana (Mitchell, 1993; Mitchell and Arthur, 2014). The available palaeoclimatic and archaeological data (i.e., Zohar and Cooke, 1997; Roberts et al., 2013) suggests that the shift toward a wetter, but more variable, climate in the summer rainfall region during the terminal Pleistocene and early Holocene greatly ameliorated conditions west of the Maloti-Drakensberg Escarpment, attracting hunter-gatherers after a long period of relatively sparse population. At this time, a single *Nerita* marine shell bead, whose distribution includes the Pondoland coastline ~200 km to the east, makes its first appearance in the Sehonghong sequence (ca. 14–15 ka).

A vervet monkey (*Chlorocebus pygerythrus*) scapula has also been documented from Sehonghong layer BAS dating to 24.5–22.8 ka during the early LGM. It is unlikely that a woodland-adapted species was present in highland Lesotho during this time (Plug and Mitchell, 2008). At Waterfall Bluff, the presence of an ostrich eggshell bead (CN26816) from SRCS Josh also provides evidence for the movement of objects from inland to the coast during the Middle Holocene, assuming that the current distribution of ostriches—which are not indigenous to Pondoland today—was similar in the past (Cooper et al., 2009). Together, the marine and ostrich shell beads, as well as exotic faunal remains, hint at persistent contacts between coastal Indian Ocean and hinterland contexts, either through exchange via extensive social networks or group movement (Mitchell, 1996). Future studies at Waterfall Bluff will enable us to shed light on possible connections between coastal foraging groups and those located at more inland regions.

More broadly, we can look at the technology to assess how the LBCS and SRCS assemblages fit into the regional culture-history framework (Lombard et al., 2012). The LBCS emphasis on small elongated flake production and the single platform-on-anvil bladelet core would align the assemblage with others labeled “Robberg” at sites such as Sehonghong, Melikane, Rose Cottage Cave, and Umhlatuzana (Deacon, 1984; Wadley, 1991; Mitchell, 1996; Low and Mackay 2016; Porraz et al., 2016; Low, 2019). However, high retouch frequencies in the LBCS suggest a point of departure from

some Robberg assemblages elsewhere (cf. Deacon, 1984) and add to a growing understanding of technological variability within Robberg assemblages (Low, 2019). This should come as no surprise as Waterfall Bluff represents the first directly dated evidence for coastal foraging during the LGM with the associated technological adaptations having no prior referents in the local archaeological record. However, this pattern could also be a result of our limited sample size and will need to be assessed in future work on a larger lithic sample.

The SRCS lithic patterns are more directly associated with the ‘Oakhurst’ or late Pleistocene / early Holocene non-microlithic techno-complexes defined elsewhere at sites such as Rose Cottage Cave, Ha Makotoko, and Ntloana Tšoana by the emphasis on larger (>50 mm in maximum dimension) side-struck flakes, an assortment of scrapers (convex edges >45°), backed and naturally backed knives (straight edges <45°), adzes, irregular or informal multiplatform cores, and worked bone (Deacon, 1984). Absent from the SRCS assemblage are the Oakhurst’s smaller (<40 mm in maximum dimension) convex scraper forms typically referred to as “Woodlot” or “duck-billed” scrapers that are characteristic of many similarly aged assemblages in Lesotho and on the south coast (Deacon, 1984; Mitchell, 1993). Use-wear analyses show some of these tool types were used for specialized tasks such as woodworking and preparing hides, and their absence at Waterfall Bluff could reflect the lack of such tasks. It should also be mentioned that Goodwin and Van Riet Lowe (1929) contended that scraper size variants were time-dependent; thus, larger scrapers occurred earlier in Oakhurst assemblages than smaller scrapers. One notable point of departure between the SRCS materials and other Oakhurst assemblages in southern Africa is the use of small water-worn hornfels cobbles for miniaturized flake production. This pattern suggests an opportunistic form of raw material procurement embedded with shellfish foraging strategies that has never before been documented. It also implies a close association between the coastline and lithic technological organization.

The hunter-gatherer occupants at Waterfall Bluff exhibited lithic technologies that have similarities to assemblages produced elsewhere in southern Africa across the late Pleistocene and Early Holocene, albeit with idiosyncrasies whose meanings are not yet fully understood. It is particularly intriguing that archaeological records in Lesotho are absent during the peak LGM while Waterfall Bluff now provides direct evidence that people were occupying the coastline. If, and how, those people at Waterfall Bluff were related to hunter-gatherers occupying the Lesotho highlands or other areas surrounding Pondoland remains to be seen. Yet, there is enough evidence to hypothesize links between the coastal lowlands and highlands.

## CONCLUSION

Excavations by the P5 Project at Waterfall Bluff provide a new and rich data archive about hunter-gatherer occupations and behaviors from an under-studied part of southern Africa. Our multi-proxy paleoenvironmental data show varying but

sustained moisture and presence of all major vegetation types found in the region today (e.g., forests, grasslands, etc.) from the end of the Pleistocene to the Holocene (Esteban et al., 2019). These data are linked with our high-resolution archaeological excavations, described here, to understand hunter-gatherer behavior in a persistent coastal context across a glacial/interglacial boundary.

Excavations at Waterfall Bluff have thus far revealed a complex but well-preserved stratigraphic sequence. Our robust and multi-proxy dating strategy has further demonstrated that hunter-gatherers visited the site throughout MIS 3, the LGM, the LGIT, and the Early Holocene with no evidence for substantial occupation hiatuses. There were also occupations during the Middle Holocene. We have coupled this detailed chronology to an equally robust sampling and analytical protocol that is beginning to yield new insights into the prehistoric contexts and behaviors of the hunter-gatherer groups who visited the site. Furthermore, the occurrence of shellfish and marine fish remains throughout the archaeological record at Waterfall Bluff makes this site unique in southern Africa, where evidence for marine exploitation from all other contemporaneous sites ends ~30,000 years ago and does not return until ~14,000 years ago.

Yet coastal resources at Waterfall Bluff do not appear to have been prioritized over any others. Instead, the central location of Waterfall Bluff between the coast and the surrounding landscape may have been the site’s main draw, as hunter-gatherers moved throughout the landscape exploiting various resources. The site’s occupation patterns align with regional site occupation trends across the LGM and Early Holocene suggesting broader region-wide processes linking coastal and inland hunter-gatherer groups. Further work will continue using multiple strands of evidence to elucidate various details about the variability of forager lifeways during the LGM and Early Holocene and will also aim at situating Waterfall Bluff within possible larger demographic and mobility patterns across the Eastern Cape and Maloti-Drakensburg escarpment.

## ACKNOWLEDGMENTS

The P5 project thanks King Zanozuko Tyelovuyo Sigcau of AmaMpondo and the hospitality of the AmaMpondo people. The project further acknowledges the inestimable support of Nkosi Mthuthuzeli Mkwedini and the Lambasi AmaMpondo community for their continued interest in our research at Waterfall Bluff. P5 also thanks Lungiswa Sihlobo of the Ingquza Hill Municipality and local tourism associations for their support throughout the broader region and in promoting ecotourism at the site. We also want to acknowledge Sello Mokhanye and the Eastern Cape Provincial Heritage Resources Authority, Phillip Hine and the South African Heritage Resources Authority, Kevin Cole and the East London Museum, Celeste Booth and the Albany Museum of South Africa, and John Costello and Kathryn Costello. IE acknowledges the Department of Science and Technology - National Research Foundation Centre of Excellence in Palaeosciences. ECF acknowledges the support of Imatest, LLC for complimentary use of Imatest 5 software. AO and KS acknowledge use of the facilities at the University of

Wollongong Electron Microscopy Centre and the assistance of Tony Romeo and Mitchell Nancarrow. IZ acknowledges the assistance of Qurban Rouhanni and the South African Institute of Aquatic Biology. RBS acknowledges the support of the Australian Government Research Training Program Scholarship. The field research was made possible through the support of a grant from the US National Science Foundation (BCS-1827326 to Fisher, Cawthra, Esteban, and Pargeter). Excavations at Waterfall Bluff were conducted under the auspices of the Eastern Cape Provincial Heritage Resources Authority, permit #2/2/APM-PERMIT/15/03/001-.

## SUPPLEMENTARY MATERIAL

The supplementary materials for this article can be found at <https://doi.org/10.1017/qua.2020.26>.

## REFERENCES

- Aitken, M.J., 1998. *An Introduction to Optical Dating*. Oxford University Press, New York.
- Amante, C., Eakins, B., 2009. ETOPO1 1 arc-minute global relief model: procedures, data sources and analysis. NOAA Technical Memorandum NESDIS NGDC-24.
- Anderson, D.G., Maasch, K.A., Sandweiss, D.H., Mayewski, P.A., 2007. Chapter 1 — Climate and culture change: Exploring Holocene transitions. In: Anderson, D.G., Maasch, K.A., Sandweiss, D.H. (Eds.), *Climate Change and Cultural Dynamics*. Academic Press, San Diego, pp. 1–23.
- Bader, G., Cable, C., Lentfer, C., Conard, N., 2016. Umbeli Belli Rock Shelter, a forgotten piece from the puzzle of the Middle Stone Age in KwaZulu-Natal, South Africa. *Journal of Archaeological Science: Reports* 9, 608–622.
- Bernatchez, J.A., Marean, C.W., 2011. Total station archaeology and the use of digital photography. *SAA Archaeological Record* 11, 16–21.
- Binford, L.R., 1980. Willow smoke and dogs' tails: Hunter-gatherer settlement systems and archaeological site formation. *American Antiquity* 45, 4–20.
- Bird, D.W., Bliege Bird, R.L., 1997. Contemporary Shellfish Gathering Strategies among the Meriam of the Torres Strait Islands, Australia: Testing Predictions of a Central Place Foraging Model. *Journal of Archaeological Science* 24, 39–63.
- Bird, D.W., Richardson, J.L., Veth, P.M., Barham, A.J., 2002. Explaining shellfish variability in middens on the Meriam Islands, Torres Strait, Australia. *Journal of Archaeological Science* 29, 457–469.
- Bosman, C., 2013. *The marine geology of the Aliwal Shoal, Scottburgh, South Africa*. Ph.D. dissertation, University of Kwa-Zulu Natal.
- Bøtter-Jensen, L. and Mejdahl, V., 1988. Assessment of beta dose-rate using a GM multicounter system. *Nuclear tracks and radiation measurements* 14, 187–191.
- Bradfield, J., 2019. Fishing with gorges: Testing a functional hypothesis. *Journal of Archaeological Science: Reports* 24, 593–607.
- Branch, G.M., Griffiths, C.L., Branch, M.L., Beckley, L.E., 2010. *Two oceans: A guide to marine life of southern Africa*. D. Philip, Cape Town.
- Butler, V., 1992. *Distinguishing natural from cultural salmonid deposits in Pacific Northwest North America*. Ph.D. dissertation, University of Washington.
- Cable, C., 1984. Economy and technology in the Late Stone Age of southern Natal. BAR, Oxford.
- Cannon, D.Y., 1987. *Marine fish osteology: a manual for archaeologists*. Archaeology Press, Simon Fraser University Burnaby, British Columbia, Canada.
- Cawe, S.G., 1994. Rainfall and vegetation patterns in Transkei and environs. *South African Journal of Science* 90, 79–85.
- Cawthra, H.C., Uken, R., Ovechkina, M., 2012. New insights into the geological evolution of the Durban Bluff and adjacent Blood Reef, Durban, South Africa. *South African Journal of Geology* 115, 291–308.
- Celliers, L., Mann, B., Macdonald, A., Schleyer, M., 2007. A benthic survey of the rocky reefs off Pondoland, South Africa. *African Journal of Marine Science* 29, 65–77.
- Chandler, G., Merry, C., 2010. The South African Geoid 2010: SAGEOID10. *Position IT*, 29–33.
- Chase, B.M., Faith, J.T., Mackay, A., Chevalier, M., Carr, A.S., Boom, A., Lim, S., Reimer, P.J., 2018. Climatic controls on Later Stone Age human adaptation in Africa's southern Cape. *Journal of Human Evolution* 114, 35–44.
- Chubb, E.C., King, G.B., Mogg, A.O.D., 1934. A new variation of Smithfield culture from a cave on the Pondoland coast. *Transactions of the Royal Society of South Africa* 22, 245–267.
- Clark, P.U., Dyke, A.S., Shakun, J.D., Carlson, A.E., Clark, J., Wohlfarth, B., Mitrovica, J.X., Hostetler, S.W., McCabe, A.M., 2009. The Last Glacial Maximum. *Science* 325, 710–714.
- Collins, J.A., Carr, A.S., Schefuß, E., Boom, A., Sealy, J., 2017. Investigation of organic matter and biomarkers from Diepkloof Rock Shelter, South Africa: Insights into Middle Stone Age site usage and palaeoclimate. *Journal of Archaeological Science* 85, 51–65.
- Cooper, R., Mahrose, K.M., Horbańczuk, J., Villegas-Vizcaíno, R., Sebei, S., Mohammed, A.E., 2009. The wild ostrich (*Struthio camelus*): a review. *Tropical Animal Health and Production* 41, 1669.
- Copeland, S.R., Cawthra, H.C., Fisher, E.C., Lee-Thorp, J.A., Cowling, R.M., le Roux, P.J., Hodgkins, J., Marean, C.W., 2016. Strontium isotope investigation of ungulate movement patterns on the Pleistocene Paleo-Agulhas Plain of the Greater Cape Floristic Region, South Africa. *Quaternary Science Reviews* 141, 65–84.
- Cunningham, A.C., 2016. External beta dose rates to mineral grains in shell-rich sediment. *Ancient TL* 34, 1–5.
- Davies, O., 1976. The 'Sangoan' industries. *Annals of the South African Museum* 22, 885–911.
- Davies, O., 1982. The Paleolithic sequence at Umgababa ilmenite diggings, South Africa. *Annals of the Natal Museum* 25, 41–60.
- Deacon, J., 1984. The Later Stone Age of southernmost Africa, Cambridge monographs in African archaeology. *British Archaeological Reports International Series*. BAR, Oxford.
- Dingle, R., Birch, G.F., Bremner, J.M., De Decker, R.H., Du Plessis, A., Engelbrecht, J.C., Fincham, M.J., et al., 1987. Bathymetry Around Southern Africa (SE Atlantic & SW Indian Oceans), scale 1: 3,475,000 at Lat. 30°. University of Cape Town, Cape Town.
- Duller, G., 2004. Luminescence dating of Quaternary sediments: recent advances. *Journal of Quaternary Science* 19, 183–192.
- Duncan, R.A., Hooper, P., Rehacek, J., Marsh, J., Duncan, A., 1997. The timing and duration of the Karoo igneous event,

- southern Gondwana. *Journal of Geophysical Research: Solid Earth* 102, 18127–18138.
- Eagles, G., 2007. New angles on South Atlantic opening. *Geophysical Journal International* 168, 353–361.
- Esteban, I., Bamford, M., Miller, C., Neumann, F.H., Schefuß, E., Zabel, M., Pargeter, J., Cawthra, H.C., Fisher, E.C., 2019. 22nd Conference of the Southern African Society for Quaternary Research. South Africa; Mossel Bay, South Africa.
- Faith, J.T., 2013. Taphonomic and paleoecological change in the large mammal sequence from Boomplaas Cave, western Cape, South Africa. *Journal of Human Evolution* 65, 715–730.
- Faith, J.T., 2014. Late Pleistocene and Holocene mammal extinctions on continental Africa. *Earth-Science Reviews* 128, 105–121.
- Feely, J.M., 1980. Did Iron Age man have a role in the history of Zululand's wilderness landscapes. *South African Journal of Science* 76, 150–152.
- Feely, J.M., 1985. Smelting in the Iron Age of Transkei. *South African Journal of Science* 81, 10–11.
- Feely, J.M., 1986. *The distribution of Iron Age farming settlement in Transkei, 470 to 1870*. University of Natal.
- Feely, J.M., Bell-Cross, S.M., 2011. The distribution of Early Iron Age settlement in the Eastern Cape: Some historical and ecological implications. *South African Archaeological Bulletin* 66, 105–112.
- Fisher, E.C., 2016. The P5 Project: Research questions, current results and future directions. *The Digging Stick* 33, 1–5.
- Fisher, E.C., Akkaynak, D., Harris, J., Herries, A.I.R., Jacobs, Z., Karkanas, P., Marean, C.W., McGrath, J.R., 2015. Technical considerations and methodology for creating high-resolution, color-corrected, and georectified photomosaics of stratigraphic sections at archaeological sites. *Journal of Archaeological Science* 57, 380–394.
- Fisher, E.C., Albert, R.-M., Botha, G., Cawthra, H.C., Esteban, I., Harris, J., Jacobs, Z., et al., 2013. Archaeological reconnaissance for Middle Stone Age sites along the Pondoland Coast, South Africa. *PaleoAnthropology*, 104–137.
- Fisher, E.C., Bar-Matthews, M., Jerardino, A., Marean, C.W., 2010. Middle and Late Pleistocene paleoscape modeling along the southern coast of South Africa. *Quaternary Science Reviews* 29, 1382–1398.
- Flemming, B., 1981. Factors controlling shelf sediment dispersal along the southeast African continental margin. *Marine Geology* 42, 259–277.
- Galbraith, R.F., Roberts, R.G., Laslett, G.M., Yoshida, H., Olley, J.M., 1999. Optical dating of single and multiple grains of quartz from Jinmium rock shelter, northern Australia, part 1: Experimental design and statistical models. *Archaeometry* 41, 339–364.
- Goodwin, A.J.H., van Riet Lowe, C., 1929. The Stone Age Cultures of South Africa. *Annals of the South African Museum*.
- Granadeiro, J., Silva, M., 2000. The use of otoliths and vertebrae in the identification and size-estimation of fish in predator-prey studies. *Cybium* 24, 383–393.
- Granger, J.E., Hall, M., McKenzie, B., Feely, J.M., 1985. Archaeological research on plant and animal husbandry in Transkei. *South African Journal of Science* 81, 12–15.
- Grayson, D.K., 1984. *Quantitative Zooarchaeology*. Academic Press, New York.
- Hendey, Q.B., Volman, T.P., 1986. Last interglacial sea levels and coastal caves in the Cape Province, South Africa. *Quaternary Research* 25, 189–198.
- Heroy, D.C., Anderson, J.B., 2007. Radiocarbon constraints on Antarctic Peninsula Ice Sheet retreat following the Last Glacial Maximum (LGM). *Quaternary Science Reviews* 26, 3286–3297.
- Hogg, A.G., Hua, Q., Blackwell, P.G., Niu, M., Buck, C.E., Guilderson, T.P., Heaton, T.J., et al., 2016. SHCal13 Southern Hemisphere Calibration, 0–50,000 Years cal BP. *Radiocarbon* 55, 1889–1903.
- Huntley, D.J., Godfrey-Smith, D.I., Thewalt, M.L.W., 1985. Optical dating of sediments. *Nature* 313, 105–107.
- Jacobs, Z., Wintle, A.G., Roberts, R.G., Duller, G.A.T., 2008. Equivalent dose distributions from single grains of quartz at Sibudu, South Africa: Context, causes and consequences for optical dating of archaeological deposits. *Journal of Archaeological Science* 35, 1808–1820.
- Jerardino, A., 1997. Changes in shellfish species composition and mean shell size from a late-Holocene record of the west coast of southern Africa. *Journal of Archaeological Science* 24, 1031–1044.
- Jerardino, A., 2016a. On the origins and significance of Pleistocene coastal resource use in southern Africa with particular reference to shellfish gathering. *Journal of Anthropological Archaeology* 41, 213–230.
- Jerardino, A., 2016b. Shell density as proxy for reconstructing prehistoric aquatic resource exploitation, perspectives from southern Africa. *Journal of Archaeological Science: Reports* 6, 637–644.
- Jerardino, A., 2017. Water-worn shell and pebbles in shell middens as proxies of palaeoenvironmental reconstruction, shellfish procurement and their transport: A case study from the West Coast of South Africa. *Quaternary International* 427, 103–114.
- Jerardino, A., 2018. *Shell Fragmentation Beyond Screen-Size and the Reconstruction of Intra-Site Settlement Patterns: A Case Study from the West Coast of South Africa*. In: Giovias, C., LeFebvre, M. (Eds.), *Zooarchaeology in Practice: Case Studies in Methodology and Interpretation in Archaeofaunal Analysis*. Springer, pp. 151–171.
- Jerardino, A., Navarro, R., 2008. Shell morphometry of seven limpet species from coastal shell middens in southern Africa. *Journal of Archaeological Science* In Press, Corrected Proof.
- Johnson, M., Karpeta, W., 1979. Geological map series of South Africa, 1:250,000. Umtata sheet., South Africa Geological Survey. Geologic Maps 1:250,000. Council for Geoscience, Pretoria.
- Jury, M.R., Valentine, H.R., Lutjeharms, J.R.E., 1993. Influence of the Agulhas Current on summer rainfall along the southeast coast of South Africa. *Journal of Applied Meteorology* 32, 1282–1287.
- Kaplan, J., 1990. The Umhlatuzana rock shelter sequence: 100,000 years of Stone Age history. *Natal Museum Journal of Humanities* 2, 1–94.
- Karkanas, P., Brown, K.S., Fisher, E.C., Jacobs, Z., Marean, C.W., 2015. Interpreting human behavior from depositional rates and combustion features through the study of sedimentary microfacies at site Pinnacle Point 5–6, South Africa. *Journal of Human Evolution* 85, 1–21.
- Keller, H.M., Hodgkins, J.M., Cleghorn, N.E., 2019. Nutritional stress and marine exploitation: Subsistence strategies at KEH-1, South Africa, during the Middle and Later Stone Age transition, Paleoanthropology Society Meeting Abstracts, Albuquerque, NM, 9–10 April, 2019. *Paleoanthropology*, Albuquerque, NM.
- Kilburn, R., Rippey, E., 1982. *Sea shells of southern Africa*. Macmillan, Johannesburg.
- Kingsley, C.S., Marshall, C.G.A., 2009. Lithostratigraphy of the Msikaba formation (Cape Supergroup). South African Council for Geoscience, Lithographic Series, No. 50, Pretoria.

- Kirch, P.V., 2005. Archaeology and global change: The Holocene Record. *Annual Review of Environment and Resources* 30, 409–440.
- Klein, R.G., 1972. The late Quaternary mammalian fauna of Nelson Bay Cave (Cape Province, South Africa): Its implications for megafaunal extinctions and environmental and cultural change. *Quaternary Research* 2, 135–142.
- Klein, R.G., 1976. The mammalian fauna of the Klasies River Mouth sites, southern Cape Province, South Africa. *South African Archaeological Bulletin* 31, 75–98.
- Kuman, K., Clarke, R.J., 2005. *The Red Sands: KwaZulu-Natal and Transkei Coast near Port Edwards, Report on a research visit, 4 to 11 September, 2005*, University of Witwatersrand.
- Lawes, M.J., Eeley, H.A.C., Findlay, N.J., Forbes, D., 2007. Resilient forest faunal communities in South Africa: a legacy of palaeoclimatic change and extinction filtering? *Journal of Biogeography* 34, 1246–1264.
- Loftus, E., Pargeter, J., Mackay, A., Stewart, B., Mitchell, P., 2019. Late Pleistocene human occupation in the Maloti-Drakensberg region of southern Africa: New radiocarbon dates from Rose Cottage Cave and inter-site comparisons. *Journal of Anthropological Archaeology* 56.
- Lombard, M., Wadley, L., Deacon, J., Wurz, S., Parsons, I., Mohapi, M., Swart, J., Mitchell, P., 2012. South African and Lesotho Stone Age sequence updates (I). *South African Archaeological Bulletin* 67, 123–140.
- Low, M., 2019. Continuity, Variability and the Nature of Technological Change During the Late Pleistocene at Klipfonteinrand Rockshelter in the Western Cape, South Africa. *African Archaeological Review* 36, 67–88.
- Low, M., Mackay, A., 2016. The late Pleistocene microlithic at Putslaagte 8 rockshelter in the Western Cape, South Africa. *South African Archaeological Bulletin* 71, 146–159.
- Maggs, J., 2011. *Fish surveys in exploited and protected areas of the Pondoland Marine Protected Area with consideration of the impact of the MPA on coastal fisheries*. Ph.D. dissertation, University of KwaZulu-Natal, Durban.
- Maggs, J., Mann, B., Cowley, P., 2013. Contribution of a large no-take zone to the management of vulnerable reef fishes in the South-West Indian Ocean. *Fisheries Research* 144, 38–47.
- Marean, C.W., 2016. The transition to foraging for dense and predictable resources and its impact on the evolution of modern humans. *Philosophical Transactions of the Royal Society B: Biological Sciences* 371, 2015.0239.
- Marean, C.W., Bar-Matthews, M., Bernatchez, J., Fisher, E., Goldberg, P., Herries, A.I.R., Jacobs, Z., et al., 2007. Early human use of marine resources and pigment in South Africa during the Middle Pleistocene. *Nature* 449, 905–908.
- Martin, A.K., Flemming, B.W., 1987. Aeolianites of the South African coastal zone and continental shelf as sea-level indicators. *South African Journal of Science* 83, 507–508.
- Martin, A.K., Hartnady, C., 1986. Plate tectonic development of the South West Indian Ocean: A revised reconstruction of East Antarctica and Africa. *Journal of Geophysical Research: Solid Earth* 91, 4767–4786.
- Mbele, V., Mullins, S., Winkler, S., Woodborne, S., 2017. Acceptance Tests for AMS Radiocarbon Measurements at iThemba LABS, Gauteng, South Africa. *Physics Procedia* 90, 10–16.
- McQuaid, C., Lindsay, J., Lindsay, T., 2000. Interactive effects of wave exposure and tidal height on population structure of the mussel *Perna perna*. *Marine Biology* 137, 925–932.
- Mitchell, P., 1988. The early microlithic assemblages of southern Africa. *British Archaeology Series*. BAR, Oxford.
- Mitchell, P., 1993. Archaeological investigations at two Lesotho rock-shelters: Terminal Pleistocene/early Holocene assemblages from Ha Makotoko and Ntloana Tsoana. *Proceedings of the Prehistoric Society*. Cambridge University Press, pp. 39–60.
- Mitchell, P., 1996. Prehistoric exchange and interaction in south-eastern southern africa: Marine shells and ostrich eggshell. *African Archaeological Review* 13, 35–76.
- Mitchell, P., Arthur, C., 2014. Ha Makotoko: Later stone age occupation across the Pleistocene/Holocene transition in western Lesotho. *Journal of African Archaeology* 12, 205–232.
- Morales Muñoz, A., Rosenlund, K., 1979. Fish Bone Measurements; An Attempt to Standardize the Measuring of Fish Bones from Archaeological Sites. *Steenstrupia*, 1–48.
- Mucina, L., Geldenhuys, C.J., 2006. Afrotemperate, subtropical, and azonal forests. In: Mucina, L., Rutherford, M.C. (Eds.), *The Vegetation of South Africa, Lesotho, and Swaziland*. South African National Biodiversity Institute, Pretoria, pp. 585–614.
- Mucina, L., Scott-Shaw, C.R., Rutherford, M.C., Camp, K.G.T., Matthews, W.S., Powrie, L.W., Hoare, D.B., 2006. Indian Ocean coastal Belt. In: Mucina, L., Rutherford, M.C. (Eds.), *The Vegetation of South Africa, Lesotho, and Swaziland*. South African National Biodiversity Institute, Pretoria, pp. 568–583.
- Murray, A.S., Wintle, A.G., 2000. Luminescence dating of quartz using an improved single-aliquot regenerative-dose protocol. *Radiation Measurements* 32, 57–73.
- Oestmo, S., Marean, C., 2014. Pinnacle Point: Excavation and Survey Methods. In: Smith, C. (Ed.), *Encyclopedia of Global Archaeology*. Springer, pp. 5955–5959.
- Opperman, H., 1984. *A report on excavations at Grassridge Rock Shelter, Sterkstroom District, Cape Province*. Fort Hare Papers 7, 391–406.
- Opperman, H., 1996. Strathalan Cave B, north-eastern Cape Province, south Africa: Evidence for human behaviour 29,000–26,000 years ago. *Quaternary International* 33, 45–53.
- Pargeter, J., Loftus, E., Mitchell, P., 2017. New ages from Sehonghong rock shelter: Implications for the late Pleistocene occupation of highland Lesotho. *Journal of Archaeological Science: Reports* 12, 307–315.
- Parkington, J., 2001. Mobility, seasonality and southern African hunter-gatherers. *South African Archaeological Review* LVI, 1–7.
- Parkington, J., 2003. Middens and moderns: shellfishing and the Middle Stone Age of the Western Cape, South Africa. *South African Journal of Science* 99, 243–247.
- Parkington, J., 2006. *Shorelines, Strandlopers and Shell Middens*. Krakadouw Trust, Cape Town.
- Parkington, J., 2012. Mussels and mongongo nuts: Logistical visits to the Cape west coast, South Africa. *Journal of Archaeological Science* 39, 1521–1530.
- Peeters, F.J.C., Acheson, R., Brummer, G.-J.A., de Ruijter, W.P.M., Schneider, R.R., Ganssen, G.M., Ufkes, E., Kroon, D., 2004. Vigorous exchange between the Indian and Atlantic oceans at the end of the past five glacial periods. *Nature* 430, 661–665.
- Penrith, M., 1970. The distribution of the fishes of the family Clinidae in southern Africa. *Annals of the South African Museum* 55 (3): 134–150
- Plug, I., Mitchell, P., 2008. Sehonghong: hunter-gatherer utilization of animal resources in the highlands of Lesotho. *Annals of the Transvaal Museum* 45, 31–53.

- Porraz, G., Igraja, M., Schmidt, P., Parkington, J., 2016. A shape to the microlithic Robberg from Elands Bay Cave (South Africa). *Southern African Humanities* 29, 203–247.
- Pretorius, L., Green, A., Cooper, J., Hahn, A., Zabel, M., 2019. Outer-to inner-shelf response to stepped sea-level rise: Insights from incised valleys and submerged shorelines. *Marine Geology*, 105979.
- Price, S.F., Conway, H., Waddington, E.D., 2007. Evidence for late Pleistocene thinning of Siple Dome, West Antarctica. *Journal of Geophysical Research: Earth Surface* 112, <https://doi.org/10.1029/2006JF000725>.
- Puchegger, S., Rom, W., Steier, P., 2000. Automated evaluation of <sup>14</sup>C AMS measurements. *Nuclear Instruments and Methods in Physics Research Section B: Beam Interactions with Materials and Atoms* 172, 274–280.
- Purcell, C., 2014. *Investigations of the warm and cold water route ocean gateways on glacial-interglacial and millennial timescales*. Ph.D. dissertation, Cardiff University.
- Ramsey, C., 2009a. Bayesian analysis of radiocarbon dates. *Radiocarbon* 51, 337–360.
- Ramsey, C., 2009b. Dealing with outliers and offsets in radiocarbon dating. *Radiocarbon* 51, 1023–1045.
- Reitz, E.J., Wing, E.S., 1999. *Zooarchaeology*. Cambridge University Press, New York.
- Ridgway, S.A., 1998. A cladistic phylogeny of the family Patellidae (Mollusca: Gastropoda). *Philosophical Transactions: Biological Sciences* 353, 1645–1671.
- Roberts, P., Henshilwood, C.S., van Niekerk, K.L., Keene, P., Gledhill, A., Reynard, J., Badenhorst, S., Lee-Thorp, J., 2016. Climate, Environment and Early Human Innovation: Stable Isotope and Faunal Proxy Evidence from Archaeological Sites (98–59ka) in the Southern Cape, South Africa. *PLoS ONE* 11, e0157408.
- Roberts, P., Lee-Thorp, J.A., Mitchell, P.J., Arthur, C., 2013. Stable carbon isotopic evidence for climate change across the late Pleistocene to early Holocene from Lesotho, southern Africa. *Journal of Quaternary Science* 28, 360–369.
- Roberts, P., Stewart, B.A., 2018. Defining the ‘generalist specialist’ niche for Pleistocene Homo sapiens. *Nature Human Behaviour* 2, 542–550.
- Roberts, R.G., Jacobs, Z., Li, B., Jankowski, N.R., Cunningham, A.C., Rosenfeld, A.B., 2015. Optical dating in archaeology: thirty years in retrospect and grand challenges for the future. *Journal of Archaeological Science* 56, 41–60.
- Rojo, A.L., 1991. *Dictionary of evolutionary fish osteology*. CRC Press: New York.
- Schapera, I., 1923. Bushman arrow poisons. *Bantu Studies* 2, 199–214.
- Schumann, E.H., Cohen, A.L., Jury, M.R., 1995. Coastal sea surface temperature variability along the south coast of South Africa and the relationship to regional and global climate. *Journal of Marine Research* 53, 231–248.
- Schweitzer, F.R., Wilson, M.L., 1982. Byneskranskop 1. A Late Quaternary Living Site in the Southern Cape Province, South Africa. *Annals of the South African Museum* 88, 1–203.
- Sealy, J., Lee-Thorp, J., Loftus, E., Faith, J.T., Marean, C.W., 2016. Late Quaternary environmental change in the Southern Cape, South Africa, from stable carbon and oxygen isotopes in faunal tooth enamel from Boomplaas Cave. *Journal of Quaternary Science* 31, 919–927.
- Simon, M.H., Arthur, K.L., Hall, I.R., Peeters, F.J.C., Loveday, B.R., Barker, S., Ziegler, M., Zahn, R., 2013. Millennial-scale Agulhas Current variability and its implications for salt-leakage through the Indian–Atlantic Ocean Gateway. *Earth and Planetary Science Letters* 383, 101–112.
- Simon, M.H., Gong, X., Hall, I.R., Ziegler, M., Barker, S., Knorr, G., van der Meer, M.T., Kasper, S., Schouten, S., 2015a. Salt exchange in the Indian-Atlantic Ocean Gateway since the Last Glacial Maximum: A compensating effect between Agulhas Current changes and salinity variations? *Paleoceanography* 30, <https://doi.org/10.1002/2015PA002842>.
- Simon, M.H., Ziegler, M., Bosmans, J., Barker, S., Reason, C.J.C., Hall, I.R., 2015b. Eastern South African hydroclimate over the past 270,000 years. *Scientific Reports* 5, 18153.
- Smith, M., 1980. Marine fishes of Maputaland. In: Bruton, M.N., Cooper, K.H. (Eds.), *Studies on the Ecology of Maputaland*. Rhodes University, Grahamstown, 164–187.
- Steig, E.J., Brook, E.J., White, J.W.C., Sucher, C.M., Bender, M.L., Lehman, S.J., Morse, D.L., Waddington, E.D., Clow, G.D., 1998. Synchronous Climate Changes in Antarctica and the North Atlantic. *Science* 282, 92–95.
- Stewart, B., Mitchell, P., 2016. *Beyond the shadow of a desert: aquatic resource intensification on the roof of southern Africa. Hunter-gatherer Diversity in Prehistory*. University of Colorado Press, Boulder.
- Stewart, B., Mitchell, P., 2018. Late Quaternary palaeoclimates and human-environment dynamics of the Maloti-Drakensberg region, southern Africa. *Quaternary Science Reviews* 196, 1–20.
- Thompson, J.C., 2010. Taphonomic analysis of the Middle Stone Age faunal assemblage from Pinnacle Point Cave 13B, Western Cape, South Africa. *Journal of Human Evolution* 59, 321–339.
- Thompson, J.C., Henshilwood, C.S., 2011. Taphonomic analysis of the Middle Stone Age larger mammal faunal assemblage from Blombos Cave, southern Cape, South Africa. *Journal of Human Evolution* 60, 746–767.
- Turpie, J., Beckley, L., Katua, S., 2000. Biogeography and the selection of priority areas for conservation of South African coastal fishes. *Biological Conservation* 92, 59–72.
- van Andel, T.H., 1989. Late Pleistocene Sea Levels and the Human Exploitation of the Shore and Shelf of Southern South Africa. *Journal of Field Archaeology* 16, 133–155.
- van Erkom Schurink, C., Griffiths, C., 1993. Factors affecting relative rates of growth in four South African mussel species. *Aquaculture* 109, 257–273.
- Van Wyk, A., 1996. Biodiversity of the Maputaland centre. In: van der Maesen, L.J.G., van Medenbach de Rooy (Eds.) *The biodiversity of African Plants*. Dordrecht: Kluwer Academic Publishers, 198–207.
- Vinnicombe, P., 1976. *People of the Eland: Rock Paintings of the Drakensberg Bushmen as a Reflection of their Life and Thought*. University of Natal Press, Pietermaritzburg.
- Vogel, J., Fuls, A., Visser, E., 1986. Pretoria radiocarbon dates III. *Radiocarbon* 28, 1133–1172.
- Wadley, L., 1991. Rose Cottage Cave: background and a preliminary report on the recent excavations. *The South African Archaeological Bulletin*, 125–130.
- Wadley, L., 1993. The Pleistocene Later Stone Age south of the Limpopo River. *Journal of World Prehistory* 7, 243–296.
- Waelbroeck, C., Labeyrie, L., Michel, E., Duplessy, J.C., McManus, J.F., Lambeck, K., Balbon, E., Labracherie, M., 2002. Sea-level and deep water temperature changes derived from benthic foraminifera isotopic records. *Quaternary Science Reviews* 21, 295–305.
- Wheeler, A., Jones, A., 1976. Fish remains. In: Rogerson, A. (Ed.), *Excavations on Fuller’s Hill, Great Yarmouth*. East Anglian Archaeology report, pp. 208–224.



- Winter, A., Martin, K., 1990. Late Quaternary history of the Agulhas Current. *Paleoceanography* 5, 479–486.
- Wintle, A.G., 1997. Luminescence dating: laboratory procedures and protocols. *Radiation Measurements* 27, 769–817.
- Wintle, A.G., 2014. Luminescence dating methods. In: Holland, H.D., Turekian, K.K. (Eds.) *Treatise on Geochemistry*, Second Edition. Elsevier, pp. 17–35.
- Wright, J.B., 1971. *Bushman raiders of the Drakensberg, 1840–1870: A study of their conflict with stock-keeping peoples in Natal*. University of Natal Press, Pietermaritzburg.
- Yokoyama, Y., Esat, T.M., Thompson, W.G., Thomas, A.L., Webster, J.M., Miyairi, Y., Sawada, C., *et al.*, 2018. Rapid glaciation and a two-step sea level plunge into the Last Glacial Maximum. *Nature* 559, 603–607.
- Zohar, I., Cooke, R., 1997. The impact of salting and drying on fish bones: preliminary observations on four marine species from Parita Bay, Panama. *Archaeofauna* 6, 59–66.
- Zohar, I., Cooke, R., 2019. The role of dried fish: A taphonomical model of fish butchering and long-term preservation. *Journal of Archaeological Science: Reports* 26, 101864.
- Zohar, I., Dayan, T., Spanier, E., 1997. Predicting grey triggerfish body size from bones. *International Journal of Osteoarchaeology* 7, 150–156.